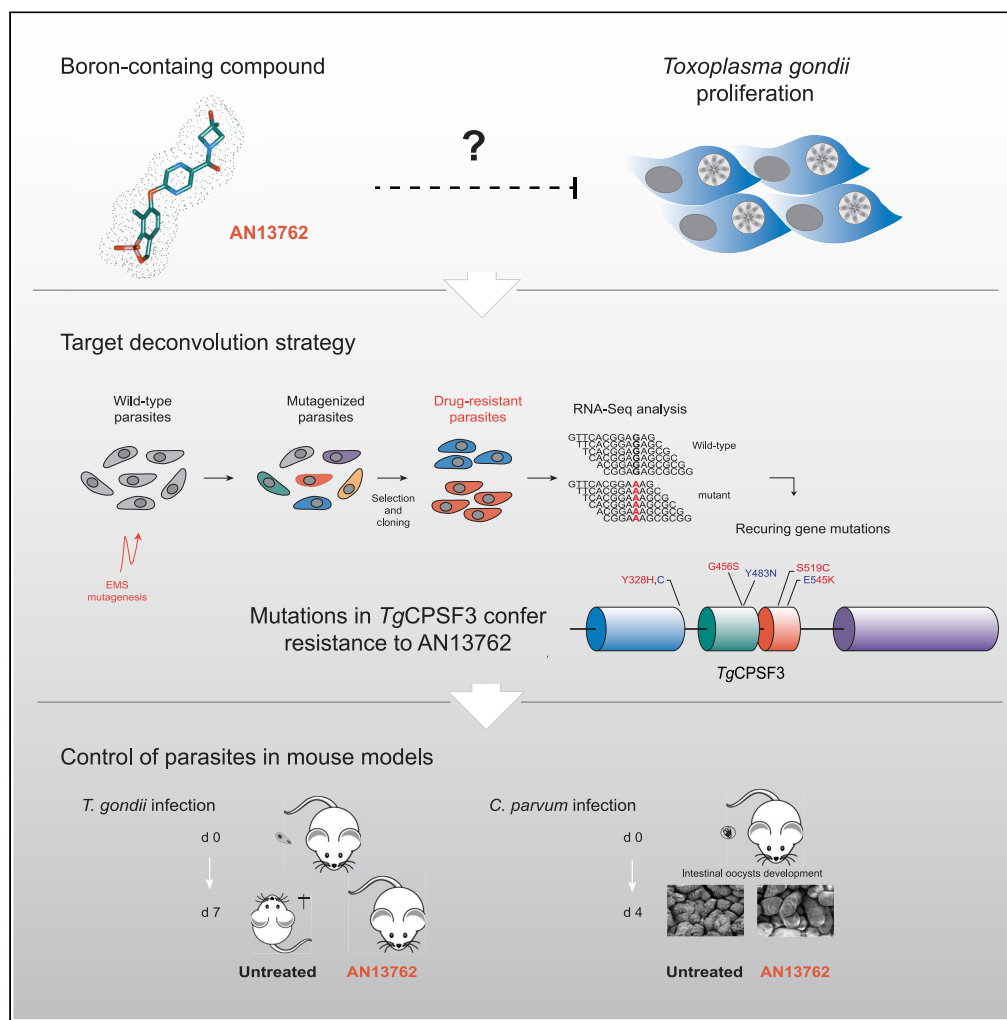


Article

Target Identification of an Antimalarial Oxaborole Identifies AN13762 as an Alternative Chemotype for Targeting CPSF3 in Apicomplexan Parasites



Valeria Bellini,
Christopher
Swale, Marie-
Pierre Brenier-
Pinchart, ...,
Fabrice Laurent,
Mohamed-Ali
Hakimi, Alexandre
Bougdour

mohamed-ali.hakimi@inserm.
fr (M.-A.H.)
alexandre.bougdour@inserm.
fr (A.B.)

HIGHLIGHTS

AN13762 is active against
T. gondii parasites

Parasites resistant to
AN13762 harbor
mutations within *TgCPSF3*

Mutations within *TgCPSF3*
confer resistance to
AN13762

AN13762 offers an
alternative for targeting
CPSF3 in *Toxoplasma* and
Cryptosporidium

Article

Target Identification of an Antimalarial Oxaborole Identifies AN13762 as an Alternative Chemotype for Targeting CPSF3 in Apicomplexan Parasites

Valeria Bellini,¹ Christopher Swale,¹ Marie-Pierre Brenier-Pinchart,¹ Tiffany Pezier,² Sonia Georgeault,³ Fabrice Laurent,² Mohamed-Ali Hakimi,^{1,4,*} and Alexandre Bougdour^{1,4,5,*}

SUMMARY

Boron-containing compounds represent a promising class of molecules with proven efficacy against a wide range of pathogens, including apicomplexan parasites. Following lead optimization, the benzoxaborole AN13762 was identified as a preclinical candidate against the human malaria parasite, yet the molecular target remained uncertain. Here, we uncovered the parasitocidal mechanisms of AN13762, by combining forward genetics with transcriptome sequencing and computational mutation discovery and using *Toxoplasma gondii* as a relevant model for Apicomplexa. AN13762 was shown to target TgCPSF3, the catalytic subunit of the pre-mRNA cleavage and polyadenylation complex, as the anti-apicomplexan benzoxaborole compound, AN3661. However, unique mutations within the TgCPSF3 catalytic site conferring resistance to AN13762 do not confer cross-protection against AN3661, suggesting a divergent resistance mechanism. Finally, in agreement with the high sequence conservation of CPSF3 between *Toxoplasma* and *Cryptosporidium*, AN13762 shows oral efficacy in cryptosporidiosis mouse model, a disease for which new drug development is of high priority.

INTRODUCTION

The Apicomplexa phylum contains intracellular single-celled parasites several of which are causative agents of animal and human diseases worldwide raising important public health problems (De Rycker et al., 2018). The group comprises important human pathogens such as *Plasmodium*, *Toxoplasma*, and *Cryptosporidium* responsible for malaria, toxoplasmosis, and cryptosporidiosis, respectively. For many of these diseases current treatments are suboptimal, and there are few or no alternatives available for some. Indeed, the current standard of treatment for *Cryptosporidium* infections, nitazoxanide, shows limited and immune-dependent effectiveness (Manjunatha et al., 2016). Although the current medication against *Toxoplasma* is quite effective, it has adverse side effects, particularly in immunocompromised patients, such as pyrimethamine-induced hematological toxicity and sulfonamide-induced skin rash, leukopenia, and thrombocytopenia (Dunay et al., 2018). In the case of malaria, emergence and spread of resistance to artemisinin-based combination therapy, the primary form of treatment, poses a constantly growing threat (De Rycker et al., 2018). Therefore, new classes of small-molecule drugs or drugs with novel modes of action are needed to overcome these limitations.

In an effort to optimize the efficacy of a novel class of boron-containing molecules against malarial parasites, the lead candidate AN13762 was identified in a phenotype-based screening (referred to as compound 46 in Zhang et al., 2017). Evaluation of pharmacokinetics showed that AN13762 has improved potency and metabolic stability, is orally bioavailable, and is equally potent across multidrug-resistant strains of *Plasmodium falciparum*, demonstrating no cross-resistance and a possible new mechanism of action. AN13762 has not exhibited either significant toxicology or cytotoxicity liabilities at any dose tested, and AN13762 was selected for preclinical development by Medicines for Malaria Venture in 2017 (Zhang et al., 2017). Although previous research on parental scaffold AN3661 identified Cleavage and Polyadenylation Specificity Factor 3 (CPSF3) as the direct target (Palencia et al., 2017; Sonoiki et al., 2017; Swale et al., 2019), a recent study investigating the resistance mechanisms of AN13762 in *P. falciparum* identified

¹Institute for Advanced Biosciences (IAB), Host-Pathogen Interactions and Immunity to Infection, INSERM U1209, CNRS UMR 5309, University Grenoble Alpes, 38000 Grenoble, France

²INRAE, Université François Rabelais de Tours, Centre Val de Loire, UMR1282 ISP, Laboratoire Apicomplexes et Immunité Mucosale, 37380 Nouzilly, France

³Plateforme des Microscopies, Université et CHRU de Tours, 37000 Tours, France

⁴These authors contributed equally to this work.

⁵Lead Contact

*Correspondence: mohamed-ali.hakimi@inserm.fr (M.-A.H.), alexandre.bougdour@inserm.fr (A.B.)

<https://doi.org/10.1016/j.isci.2020.101871>



multiple components involved in prodrug activation or sumoylation and ubiquitination pathways along with PfCPSF3 suggesting that the latter was not the primary target (Sindhe et al., 2020).

The work described here was undertaken to shed light on the parasiticidal mechanisms of AN13762 using *Toxoplasma gondii* as a relevant representative of apicomplexan parasites. Here, we present evidence that AN13762 is effective against both *T. gondii* and *Cryptosporidium parvum* *in vitro* at low micromolar concentrations and *in vivo* in mouse models of toxoplasmosis and cryptosporidiosis, respectively. Using a forward genetic approach based on transcriptome sequencing, we identified its target as CPSF3, a common target of several benzoxaboroles such as AN3661, a compound active against apicomplexan parasites (Palencia et al., 2017; Sonoiki et al., 2017; Swale et al., 2019), or the trypanocidal compounds AN11736 and acoziborole (Wall et al., 2018). Importantly, several point mutations found in *T. gondii* CPSF3 conferring resistance against AN13762 were not effective against AN3661, suggesting a divergent mode of resistance mechanisms between CPSF3 and benzoxaboroles. Hence this work uncovers the molecular mechanism for the antiparasitic activity of a preclinical antimalarial candidate AN13762 and extends the clinical spectrum of activity of this chemotype to other life-threatening apicomplexan parasites.

RESULTS

AN13762 Is Active against *T. gondii* In Vitro and In Vivo

To assess the effectiveness of AN13762 against *T. gondii* parasites, growth of the type I reference RH strain was monitored within human foreskin fibroblasts (HFFs) treated with AN13762; its parental scaffold AN3661 as a positive control (Figure 1A); pyrimethamine, the standard of care for toxoplasmosis; or vehicle (DMSO). Efficient *in vitro* inhibition of *T. gondii* growth was repeatedly confirmed, with measured half maximum effective concentration (EC₅₀) of 2.1 μM, which is almost 40 times higher than that of AN3661 (Figures 1B and 1C). Complete and sustained inhibition of growth was observed at 10 μM AN13762 without any adverse effects for the host cells (Figures 1D and S1).

When AN13762 was administered orally for 7 days to *T. gondii*-infected mice, beginning on the first day following intraperitoneal injection of parasites, 100% of the animals survived the lethal infection by the highly virulent type I RH strain in contrast to untreated controls (Figures 1E and 1F). Second lethal challenges to the mice that survived the first infection confirmed that the initial 7-day treatment with AN13762 resulted in a protective immune response to subsequent *T. gondii* infection (Figures 1E and 1F), thus strengthening the biological and pharmacokinetic profile of AN13762 in animal efficacy studies. Altogether, these results indicate that AN13762 is effective against *T. gondii* both *in vitro* and *in vivo* allowing long-term cures in mouse model of acute toxoplasmosis with comparable efficacy to current treatment.

Selection of *T. gondii* Parasites Resistant to AN13762

In an attempt to shed light on the mechanism of action of AN13762, we performed a forward genetic screen combining chemical mutagenesis to isolate AN13762-resistant parasites and next-generation sequencing analysis to map mutations conferring drug resistance (Figure 2A). Central to our approach, we reasoned that the gene(s) that would be mutated in more than one independently mutagenized resistant clone might be relevant to the drug resistance mechanism and by this means alleviating the notoriously difficult molecular mapping of point mutations induced by mutagens. For this purpose, seven independent ethyl methanesulphonate (EMS) mutagenesis experiments were performed and the resulting mutagenized parasites were selected in the presence of 10 μM AN13762 (Figure 2B), which corresponds to approximately 5-fold the EC₅₀ value. Resistant parasites were obtained from each of the seven mutagenesis experiments, whereas none of the non-mutagenized parasites survived the selection at 10 μM AN13762, attesting once more to the parasiticidal efficacy of this compound (Figure 2B). The resistant parasite lines were then cloned by limited dilution, and we selected a single clone from each mutagenesis experiment (named A1 to G1) for transcriptome sequencing by RNA sequencing (RNA-seq). All the resistant clones were able to grow and formed plaques when grown in the presence of 10 μM AN13762 (Figures 2C–2E and S2). In parallel, the parental strain was analyzed by RNA-seq and used as a reference to identify EMS-induced mutations. We use transcriptome sequencing as most drugs target expressed proteins, with levels of gene expression and mutations being part of the sequencing results.

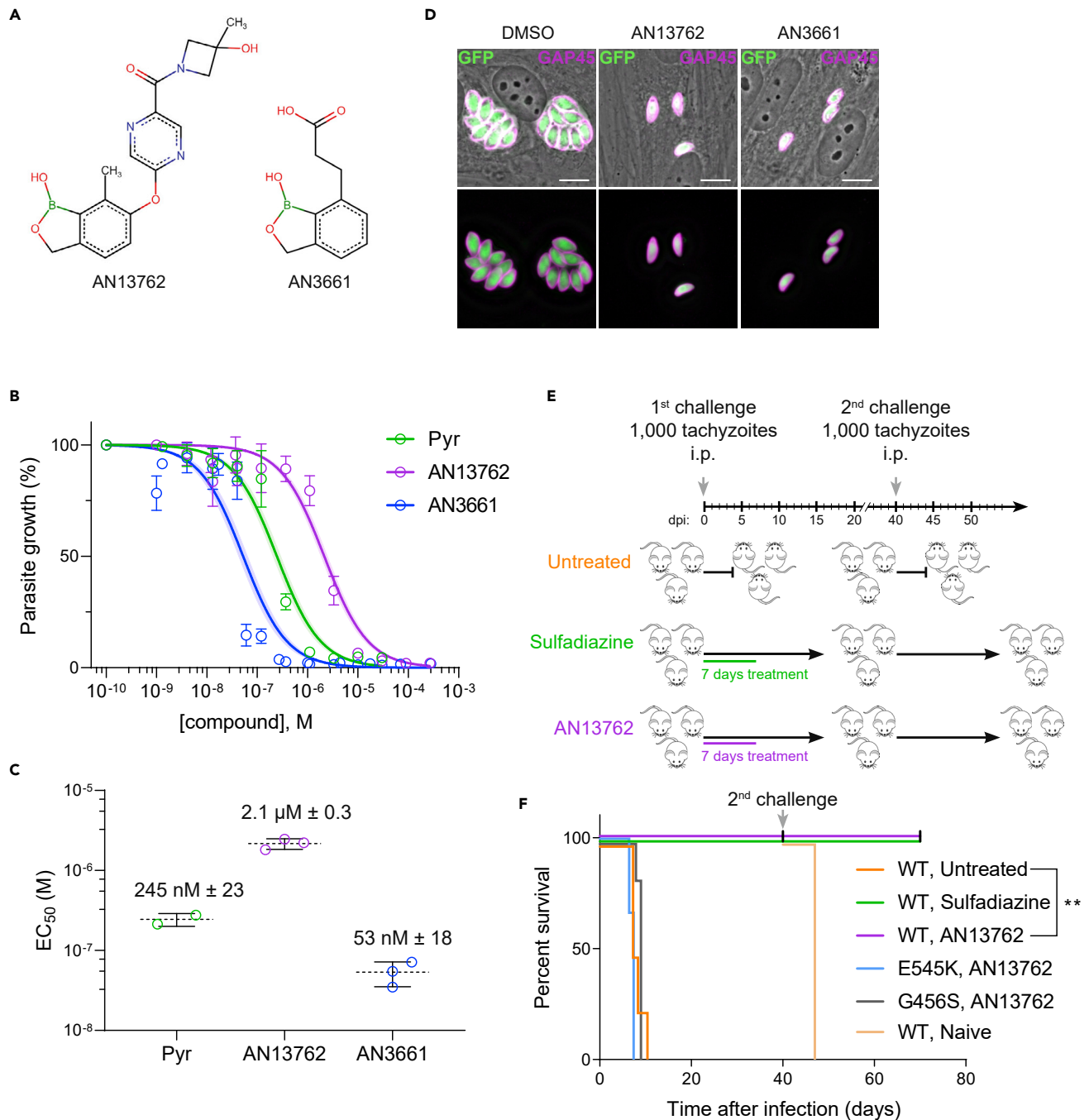


Figure 1. Activity of AN13762 against *Toxoplasma gondii*

(A) Chemical structures of benzoxaborole leads AN13762 and AN3661.

(B) Dose-response curves for inhibition of *T. gondii* growth *in vitro* in response to increasing concentration of the indicated compounds. Confluent HFF monolayer was infected with tachyzoites of *T. gondii* RH strain expressing the NanoLuc luciferase (RH $\Delta ku80$ UPRT::NLuc-P2A-EmGFP). The *T. gondii* strains used in this study are listed in Table S1. Data are presented as mean \pm standard deviation (SD) of at least two independent biological assays, each with 3 technical replicates. Shaded error envelopes depict 95% confidence intervals.

(C) EC₅₀ values of each biological replicate were determined by non-linear regression analysis. EC₅₀ data are presented as mean \pm SD from at least 2 independent biological replicates, each with 3 technical replicates.

(D) HFF cells were infected with tachyzoites (RH $\Delta ku80$ UPRT::NLuc-P2A-EmGFP) and incubated with 10 μ M AN13762, 5 μ M AN3661, or 0.1% DMSO as control. Cells were fixed 24 h post-infection and then stained with antibodies against the *T. gondii* inner membrane complex protein GAP45 (magenta). The cytosolic GFP is shown in green. Scale bars, 10 μ m. A complete dataset can be found in Figure S1.

Figure 1. Continued

(E) Acute toxoplasmosis: timeline of mouse infections and treatments. Untreated mice succumbed to infection, and thus a new group of healthy CBA/JRj mice was used for the second challenge (n = 3 in each group).

(F) Survival curves of the CBA/JRj mice infected intraperitoneally (i.p.) with 10³ tachyzoites of type I RH wild-type (WT) or the indicated *CPSF3* mutant strains (E545K or G456S). During the first challenge, mice were treated orally with 40 mg/kg AN13762 or 200 mg/kg sulfadiazine once daily beginning 1 day post-infection (n = 6 for each condition; two independent experiments, each with three mice per experimental group). Mice surviving the primary infection were challenged a second time with the *T. gondii* WT strain (second challenge). A new group of naive mice was used as control (n = 3 in each group).

Parasites Resistant to AN13762 Harbor Mutations within *TgCPSF3*

To map the EMS-induced mutations that confer drug resistance, the Illumina sequencing reads were aligned to the ~65-Mb *T. gondii* GT1 reference genome. The assembled sequences were analyzed to identify single nucleotide variations (SNVs), small insertions, or short deletions using the parental strain as a reference (see [Transparent Methods](#)). By focusing on mutations present in coding sequences, we identified a single gene, *CPSF3* (Cleavage and Polyadenylation Specific Factor 3, *TGGT1_285200*), that harbored SNVs leading to amino acid substitutions in each of the seven drug-resistant lines that were not present in the parental strain ([Figure 2F](#) and [Table 1](#)). *CPSF3* encodes a nuclear mRNA-processing endonuclease that functions in pre-mRNA maturation (Ryan, 2004), which has been previously identified as the target of several benzoxaborole compounds active against distantly related pathogens (Lunde et al., 2019; Sonoiki et al., 2017; Swale et al., 2019; Wall et al., 2018), including *T. gondii* (Palencia et al., 2017). Importantly, four different mutations were identified (G456S, E545K, Y328H, and S519C; [Figure 2G](#); [Table 1](#)), among which E545K conferred resistance against AN3661 in *T. gondii* (Palencia et al., 2017). Mutations span from the metallo-β-lactamase domain to the RNA specificity domain of *CPSF3* ([Figure 2G](#)). Therefore, these data suggest that mutations in *CPSF3* were responsible for resistance against AN13762.

Mutations within *CPSF3* Confer Resistance to AN13762

To confirm that the *CPSF3* mutations were sufficient to confer resistance to AN13762, we reconstructed each of the mutations identified in AN13762-resistant parasites into the sensitive parental wild-type strain using CRISPR/Cas9 system coupled to homology-directed repair for gene editing in *T. gondii* ([Figure 3A](#)) (Palencia et al., 2017). Thus, RHΔku80 parasites were co-transfected with a vector expressing the Cas9 endonuclease and synthetic guide RNA (sgRNA) and the corresponding homologous single-stranded donor oligonucleotides as repair template. After selection with AN13762, emerging resistant parasites were cloned, and DNA sequencing established that the mutations have been correctly inserted at *CPSF3* locus ([Figures 3B](#) and [S3A](#)). Transfections with the Cas9 control vectors alone produced no surviving parasites. In the engineered parasites, we observed that the *CPSF3* mutations E545K, G456S, S519C, and Y328H substantially decreased the sensitivity against AN13762 when compared with wild-type parasites ([Figures 3C–3E](#) and [S3B–3D](#)). It is noteworthy that Y328H mutation had a significant effect on parasite growth in the absence of drug ([Figure 3C](#), upper panel), suggesting that this mutation might affect basal activity of *CPSF3* in tachyzoites, which is in line with *CPSF3* being essential to parasite growth (Palencia et al., 2017; Sidik et al., 2016). In addition, the *CPSF3*-edited parasites harboring the mutations E545K or G456S were also resistant to AN13762 treatment in mice ([Figure 1F](#)). Altogether, these data confirm the primary role of *CPSF3* mutations in conferring resistance to AN13762 and indicate that AN13762, in a similar fashion to AN3661, targets *CPSF3* (Palencia et al., 2017; Swale et al., 2019).

AN13762-Resistant Mutations G456S and S519C Do Not Confer Cross-Resistance to AN3661

We had previously found that mutations in *CPSF3* were conferring resistance to another oxaborole compound, AN3661 ([Figure 2G](#), mutations Y328C, Y483N, and E545K, Palencia et al., 2017). To examine whether the AN13762-resistant mutations in *CPSF3* confer cross-resistance to AN3661, we assayed AN3661 against reconstructed parasites harboring *CPSF3* mutations E545K, G456S, S519C, and Y328H. As expected, the most prevalent mutation E545K that was identified in the mutagenesis experiments conducted against either AN13762 or AN3661 conferred resistance to both compounds ([Figures 3C–3E](#) and [S3B–3D](#)). Note that the increase in resistance to AN3661 was more dramatic than for AN13762 (~100- and ~3-fold increase in EC₅₀, respectively; [Figure 3D](#)). Very different results were obtained for G456S and S519C mutations, which did not allow parasite growth when exposed to 5 μM AN3661 ([Figure 3C](#)). The *CPSF3*^{G456S} mutation conferred the strongest resistance phenotype to AN13762 with a ~42-fold increase in AN13762 EC₅₀ when compared with wild-type parasites, whereas sensitivity to AN3661 remained unaffected ([Figures 3D](#) and [3E](#)). Of note, the latter mutations were not identified in the AN3661 screen, presumably reflecting their inability to protect against AN3661 at 5 μM. Conversely, the Y483N mutation identified in AN3661-resistant parasites conferred cross-resistance to

Chr.	Gene	Annotation	Position	Variant Calling							
				Parental Strain	Resistant Mutants						
				WT	A1	B1	C1	D1	E1	F1	G1
V	TGGT1_285200	CPSF3	2395898				E545K (GAG to AAG)	E545K (GAG to AAG)			E545K (GAG to AAG)
V	TGGT1_285200	CPSF3	2395976						S519C (AGC to TGC)		
V	TGGT1_285200	CPSF3	2396165		G456S (GGC to AGC)						G456S (GGC to AGC)
V	TGGT1_285200	CPSF3	2396549			Y328H (TAC to CAC)					

Table 1. Mutations Found in Candidate Gene Identified by RNA-Seq Transcriptome Analysis

Amino acid substitutions with the corresponding codons shown in parentheses are indicated for each mutagenized *T. gondii*-resistant mutant strain.

AN13762. Similarly, mutations affecting the Y328 residue of CPSF3 decreased sensitivity to both compounds (Figures 3C and 3D). Altogether, these results further confirm the role of CPSF3 mutations in drug resistance and indicate a divergent mode of resistance between AN13762 and AN3661.

Molecular Docking Suggests a Divergent Resistance Mechanism between Oxaboroles

Multiple sequence alignments show a high overall sequence conservation within the metallo- β -lactamase (MBL), Beta-Casp, and RNA specificity domains of CPSF3 within apicomplexan parasites and humans (Figure 4A). One notable difference between the apicomplexan and human enzyme is the presence of an extended loop or "apicomplexan specific insert" whose length varies from 20 to 59 residues. However, conservation of the generated resistant SNVs to AN13762 within *T. gondii* CPSF3 coding sequence is absolute across species and appears close to the catalytic residues but is never directly involved in the coordination of the catalytic zinc atoms. Next, we visualized the resistance-conferring mutations within the recently obtained structure of *Cryptosporidium* CPSF3 (ChCPSF3) in co-crystal with AN3661 (pdb id 6Q55) (Swale et al., 2019). With the assumption that AN13762 interacts with a comparable geometry as the AN3661 benzoxaborole group, notably through the boron-driven octahedral coordination of the two catalytic zinc ions, we placed the AN13762 derivative in the same plane as AN3661 (Figure 4B–4D). Through this modeling, we did not generate any clashes with CPSF3, despite the much bigger size of AN13762 (13.4 Å in length against 7 Å for AN3661). When visualizing both AN3661 and AN13762 placement with regard to the resistance-conferring mutations, two important features can be noted. First, most of the mutations found (Y328C/H, E545K, S519C, and Y483N) that rescue parasites from both compounds are not directly observed in contact with the compound-binding site. Instead, the mutated residues are generally placed on loop regions lining the interfacial cavity between the RNA specificity domain and Beta-Casp domain. These resistance-conferring mutations probably act indirectly on the compound activity through either an allosteric mechanism preventing compound binding or by modifying RNA recognition by CPSF3 as these loop regions are believed to regulate RNA access and recognition (Sun et al., 2020). Second, the G456S mutation, which exclusively rescues *T. gondii* parasites from AN13762, is observed separated to the other resistance-conferring mutations. Because of its close proximity with the AN13762 pyrazine ring and methylazetidide (2.2 Å distance), the G456S mutant probably introduces an important steric hindrance to AN13762 binding. AN3661, with a much shorter organic extension, does not come close enough for the mutation to have an effect on its binding and activity. As a result, the G456S mutant remains sensitive to AN3661 (Figure 3E).

AN13762 Is Active against *Cryptosporidium* In Vitro and In Vivo

The aforementioned data provide evidence that AN13762 targets CPSF3 enzyme. Given that it has been shown that CPSF3 is a bona fide target for inhibiting *Cryptosporidium* development (Swale et al., 2019),

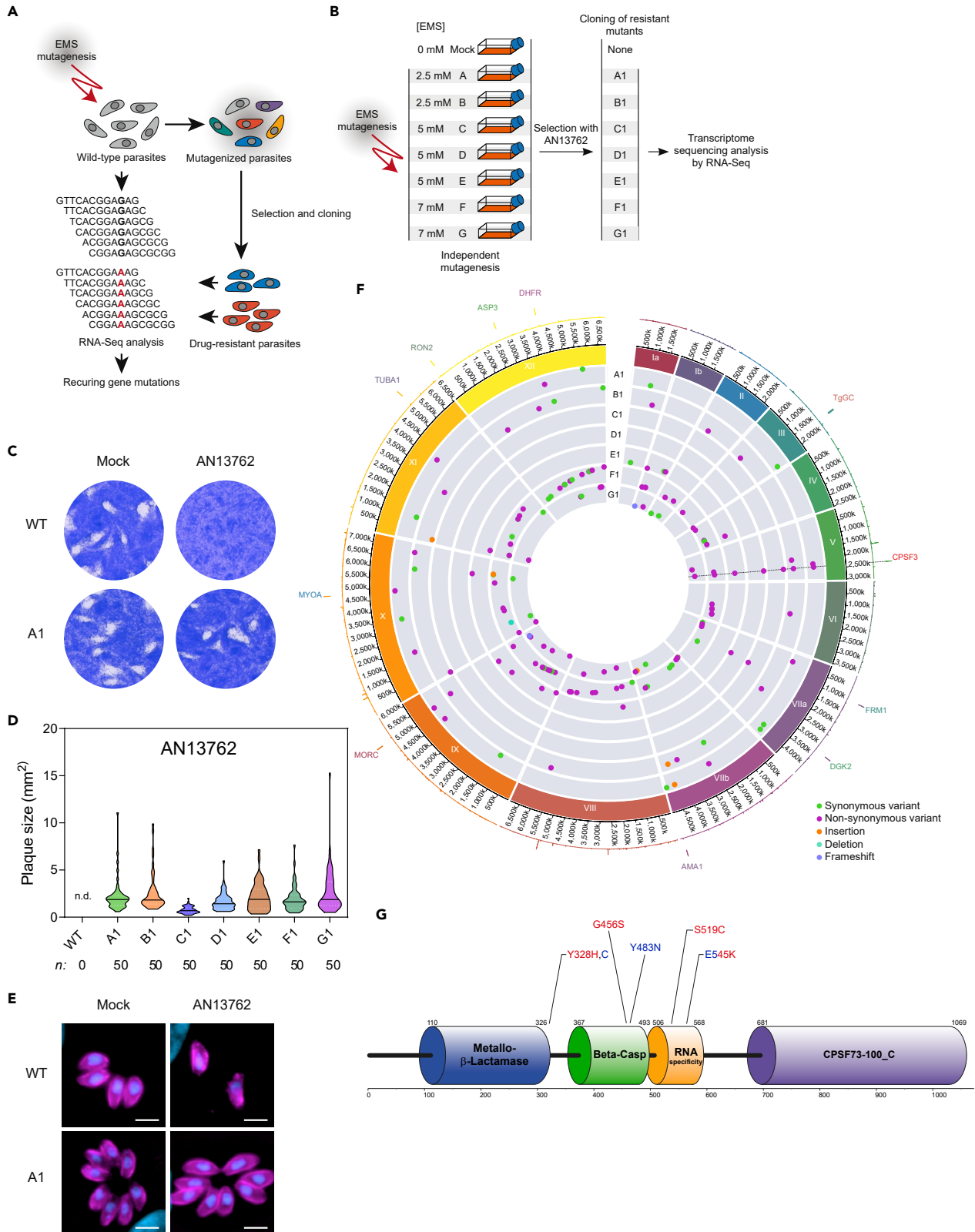


Figure 2. Strategy for AN13762 Target Deconvolution

(A) Diagram of key steps of the forward genetic screen to map mutations conferring drug resistance in *T. gondii* parasites. EMS-mutagenized population of *T. gondii* tachyzoites was selected in the presence of a lethal concentration of AN13762 to isolate drug-resistant parasites. Analysis of the parental wild-type strain and multiple resistant clones by variant-calling of sequencing reads generated by RNA-seq to identify EMS-induced mutations in coding sequences conferring drug resistance.

(B) Schematic of the strategy used to obtain *T. gondii*-resistant parasites to AN13762. From each mutagenesis experiment a single clone (A1 to F1) was isolated and analyzed by RNA-seq.

(C) AN13762-resistant parasites form plaques after 7 days of growth in the presence of 10 μ M AN13762. Complete dataset is shown in Figure S2A.

(D) Quantification of plaque sizes of wild-type parasites and resistant lines (A1 to G1) when cultured in the presence of AN13762. n.d., not detected. Associated data are shown in Figure S2C.

(E) Fluorescence microscopy showing intracellular growth of *T. gondii* AN13762-resistant lines. HFF cells were infected by the indicated *T. gondii* strains in the presence or absence of 10 μ M AN13762. At 24 h post-infection, cells were fixed and stained with antibodies against GAP45 (magenta) and Hoechst (blue) to detect the inner membrane complex (IMC) of parasites and nuclei, respectively.

(F) Circos plot summarizing single nucleotide variants (SNVs), insertions, and deletions detected by transcriptomic analysis of the *T. gondii* AN13762-resistant lines, grouped by chromosome (numbered in Roman numerals with size intervals given outside). Each dot in the seven innermost gray tracks corresponds to a scatterplot of the mutations identified in the coding regions of the seven drug-resistant strains, with each ring representing one of the seven drug-resistant lines (A1 to G1). In the second outermost track, lines depicting whole-genome RNA-seq data of the *T. gondii* parental strain (RPKM values of genes are shown). Each bar in the outermost track represents locations of selected archetypal essential genes. See Table S2 and Figure S4 for transcriptomic analysis.

(G) TgCPSF3 domain architecture as predicted from PFAM databases and crystal structures of *Cryptosporidium* CPSF3 (Swale et al., 2019). Positioning of residues that were mutated in parasites resistant to AN13762 (Y328H, G465S, S519C, and E545K, in red) or AN3661 (Y328C, Y483N, and E545K, in blue) are indicated.

we assessed the anticryptosporidial activity of AN13762 *in vitro* and *in vivo*. The ability of AN13762 to inhibit *C. parvum* INRAE Nluc fast-growing strain in human ileocecal HCT-8 was assessed with its parental scaffold AN3661 as a positive control. Although less potent than AN3661, an efficient *in vitro* inhibition of *C. parvum* growth was repeatedly observed with AN13762 (EC₅₀ 13 \pm 9 μ M) (Figures 5A, 5B and 55). AN13762 presented no detectable toxicity for the host cells, even at 100 μ M (Figure 5C). AN13762 activity was therefore assessed *in vivo* in a neonatal mouse model. Seven-day-old neonates were orally treated with AN13762 mixed in carboxymethyl cellulose (CMC) 4 h after *C. parvum* infection and daily until 3 days post-infection (dpi). Parasite load was assessed in the intestine at 4 dpi by oocyst count and measuring Nluc activity representing transgenic expression by the INRAE Nluc strain. Both methods revealed an impressive and significant inhibition of parasite development as illustrated in Figure 5D and by scanning electron microscopy where only very scarce parasites can occasionally be found on the intestinal villi of treated mice. Remarkably, the enzymatic assay revealed a 4-log reduction in luminescence signals in treated mice, and oocysts were not detected by coproscopic intestinal material examination, which is much less sensitive than the former method. Altogether, these results indicate that AN13762 is effective against *C. parvum* both *in vitro* and *in vivo* and provide an additional drug presumably acting by a different mode of action than AN3661 to block CPSF3 activity.

DISCUSSION

Whole-cell phenotypic screening is an efficient approach in drug discovery that has led to the identification of numerous antimicrobial lead compounds, although the targets and mode of action remain unknown and challenging to determine. Although clinical development remains possible without this knowledge, lack of insight into the mechanism of action is one of the biggest obstacles for further medicinal chemistry optimization or to predict and track drug resistance. Fortunately, a large variety of target deconvolution technologies are currently available. The approach developed here takes advantage of all the benefits of the EMS mutagenesis method, including its wide and mostly unbiased coverage of the genome with virtually all types of mutations (Farrell et al., 2014). In this work, by combining cost-effective RNA-seq based variant calling, computational mutation discovery and CRISPR/Cas9 genome editing, we identified CPSF3, the catalytic subunit of the pre-mRNA cleavage and polyadenylation complex, as the target of AN13762 in *T. gondii* parasites.

In eukaryotes, CPSF3 is key to the 3' end processing of both polyadenylated and replication-dependent histone precursor mRNAs (Shi and Manley, 2015). These distinct 3' ends are generated co-transcriptionally by specialized 3' end processing machineries that recognize a conserved hexanucleotide AAUAAA and a downstream G/U-rich sequence on the 3' end of nascent pre-mRNAs destined for polyadenylation or cleave histone mRNA precursors few nucleotides downstream of a highly conserved stem-loop structure (Marzluff et al., 2008). As a result, the majority of histone genes are expressed as nonpolyadenylated transcripts that

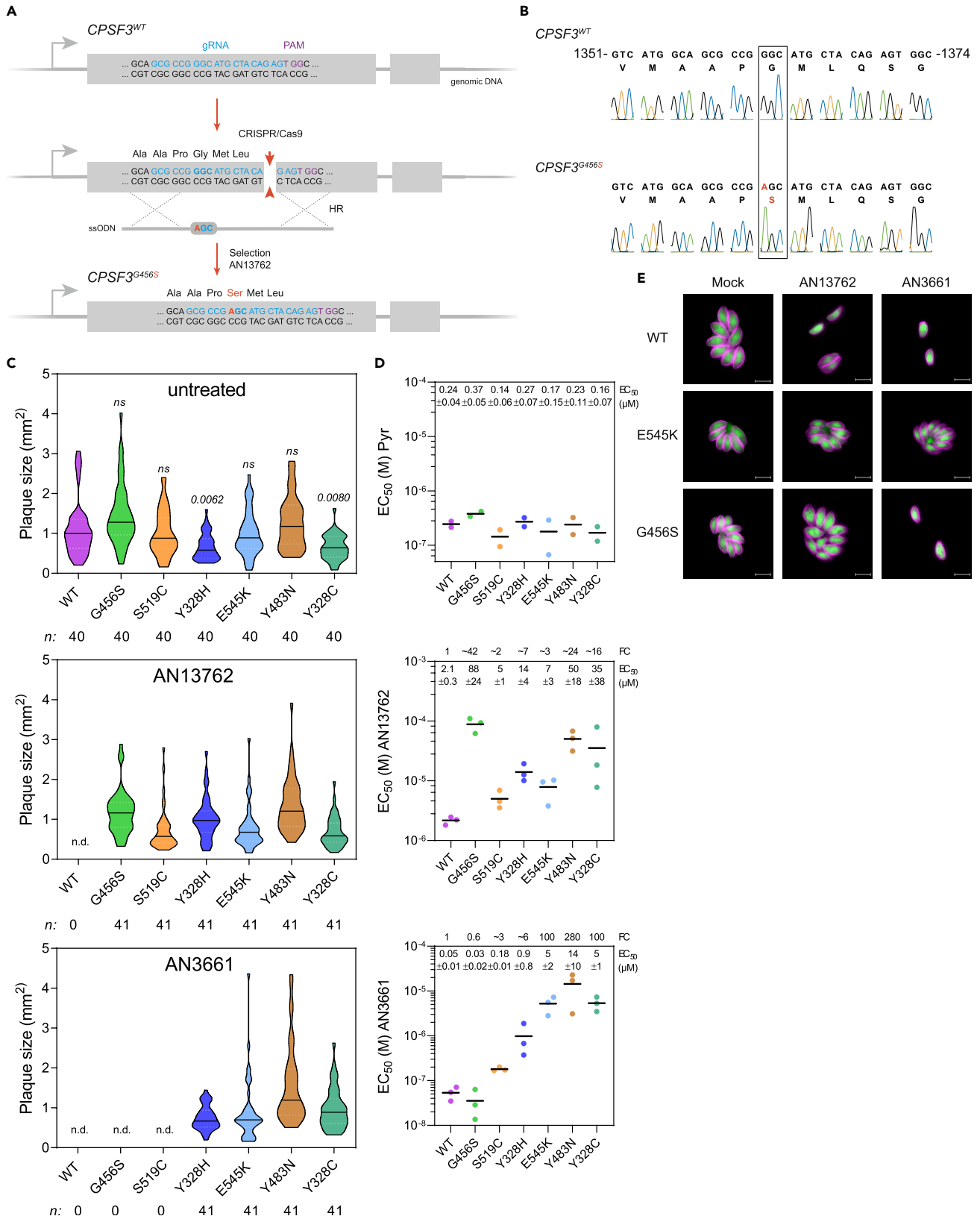


Figure 3. Validation of *T. gondii* CPSF3 as the Benzoxaborole Target

(A) Schematic of the CPSF3 gene editing strategy in *T. gondii* parasites. Detailed view of CPSF3 locus and CRISPR/Cas9-mediated homology-directed repair with single-stranded oligo DNA nucleotides (ssODNs) carrying nucleotide substitutions (orange letters). After homologous recombination (HR) events with ssODNs, CPSF3 recombinants were selected with AN13762.

(B) Sanger sequencing validation of CPSF3 editing. Chromatograms of CPSF3 DNA sequences from parental and engineered parasites are shown. Nucleotide positions relative to the ATG start codon on genomic DNA are indicated. A complete dataset can be found in Figure S3A.

(C) Effects of CPSF3 mutations on *T. gondii* lytic cycle as determined by plaque assay. Plaque sizes were measured for WT and the engineered CPSF3 mutant strains (G456S, S519C, Y328H, E545K, Y483N, Y328C) after 7 days of growth in the absence or presence of 10 μ M AN13762 or 5 μ M AN3661. n.d., not detected. p values corresponding to Kruskal-Wallis test with Dunn's multiple comparisons with the wild-type (WT) strain are indicated. ns, not significant. Associated data are shown in Figure S3B.

(D) EC₅₀ values for pyrimethamine (Pyr), AN13762, and AN3661 were determined for WT and the engineered CPSF3 mutant strains (G456S, S519C, Y328H, E545K, Y483N, Y328C). Data are mean from at least 2 independent biological replicates, each with 3 technical replicates. Associated dose-response curves are shown in Figure S3C. Mean EC₅₀ values \pm SD with fold changes (FC) in EC₅₀ relative to that of the WT parasites are indicated.

(E) Fluorescence microscopy showing intracellular growth of WT and the CPSF3-edited parasites (G456S and E545K). HFF cells were infected with tachyzoites of the indicated *T. gondii* strains expressing the *NLuc-P2A-EmGFP* reporter gene and incubated with 10 μ M AN13762, 5 μ M AN3661, or 0.1% DMSO as control. Cells were fixed 24 h post-infection and then stained with antibodies against the *T. gondii* inner membrane complex protein GAP45 (magenta). The cytosolic GFP is shown in green. Scale bars, 10 μ m. Complete dataset in shown in Figure S3D.

are poorly detected by poly(A) purification-based RNA-seq (Lyons et al., 2016; Zhao et al., 2018). Despite this technical bias, our transcriptomic data indicate that histone mRNAs (e.g., H2Ba, H4, H2Ax, H2A1, and H2Bb; Table S2 and Figure S4) were dramatically enriched in drug-resistant lines harboring CPSF3 mutations Y328H, E545K, and S519C, but not in those mutants containing the CPSF3^{G456S} allele (strains A1 and F1 in Table 1). This suggests hypomorphic mutations of CPSF3 that retain sufficient activity to overcome lethality but somehow favor histone pre-mRNA processing toward polyadenylation of transcripts that were otherwise barely detected using our poly(A)-selected transcript experiment settings. Interestingly, the mutations Y328H, E545K, and S519C are lining the channel accommodating the RNA substrate on CPSF3 (Figure S6), whereas the G456S mutation that is observed distant from the other mutations did not affect histone mRNA accumulation. It is noteworthy that the Y328 mutations significantly impacted the overall growth fitness (Figure 3C), suggesting a default in TgCPSF3^{Y328H/C} activity. As the G456S mutation in *T. gondii* is equivalent to the G330S mutation found in the human CPSF3 counterpart conferring resistance against the anti-cancer agent JTE-607 (Ross et al., 2020), it is likely that the mechanism of resistance is shared. Possibly, the G330S and G456S mutations can only be effective for elongated molecules to clash with the compound thereby impeding binding without affecting recognition of the substrate. Yet further studies are required to determine whether the mutations in CPSF3 affect the access of the substrate to the catalytic site, complex assembly, or its conformational dynamics as shown recently by Sun et al. (2020). Altogether, these results underscore the advantage of using transcriptome sequencing to investigate mechanisms of drug action and to provide functional insight into the molecular biology of the target protein.

In mammalian cells, CPSF3 is embedded in a large multisubunit complex including CPSF1, CPSF2, CPSF4, CPSF7, cleavage stimulatory factor 1 (CSTF1), CSTF2, CSTF3, symplekin, and WDR33 (Dominski and Marzluff, 2007; Ryan, 2004). A quite similar complex was purified in *T. gondii* (Table S2, Swale et al., manuscript in preparation), and the identified subunits were all predicted to be essential for tachyzoite growth *in vitro* (Sidik et al., 2016). No mutations with significant enrichment were found in the CPSF3 protein partners in the resistant strains, which is in agreement with our docking model based on *Cryptosporidium hominis* CPSF3 structural data where the oxaboroles are enfolded within the CPSF3 scaffold, presumably precluding any interaction with other components.

The mutations conferring resistance to AN13762 target TgCPSF3 catalytic site, a gold standard evidence for target confirmation of a bioactive small molecule. In the published structure of AN3661 bound to ChCPSF3, the oxaborole competes with the catalytic water molecules for zinc atoms, hence blocking the phosphate bond cleavage of the pre-mRNA substrate (Swale et al., 2019). Given the overall conservation of CPSF3 catalytic core in Apicomplexa and the high conservation of the residues involved in drug resistance, it is likely that AN13762 binds to this site and disrupts the pre-mRNA processing activity of TgCPSF3 that is essential for parasite growth.

Although it is clear that AN13762 targets CPSF3 in *T. gondii*, different results were observed in *P. falciparum* where the mechanism of resistance is plural (Sindhe et al., 2020). In fact, while we were investigating the mechanism of action of AN13762 in *T. gondii*, Sindhe and colleagues have shown that *P. falciparum*

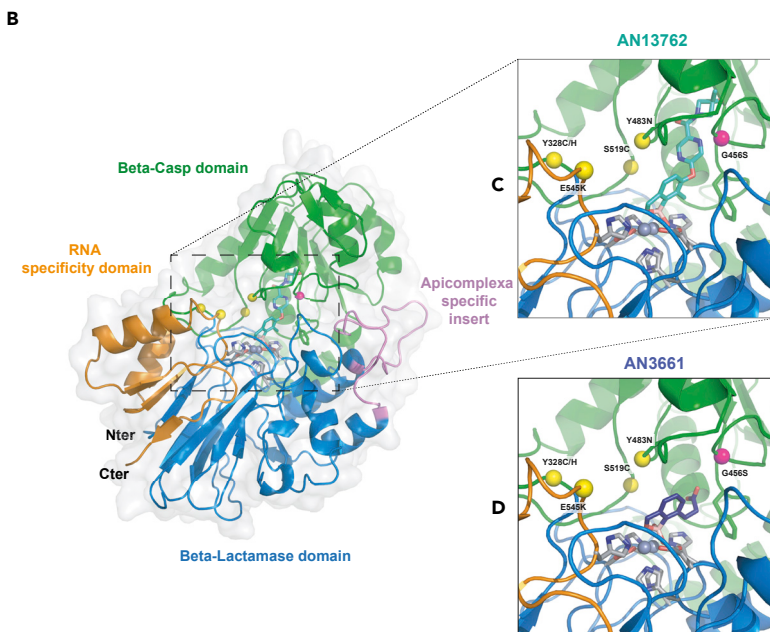
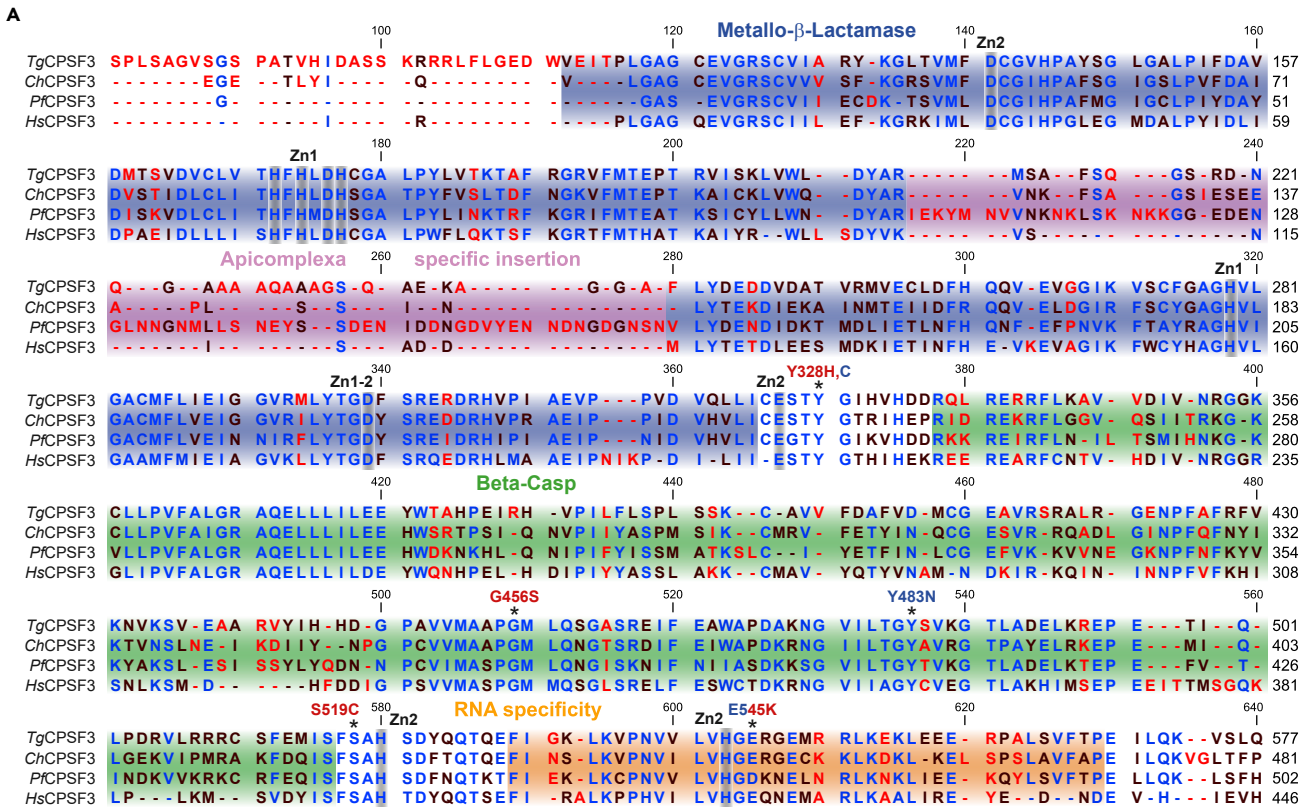


Figure 4. Docking Studies for Chemotypes AN13762 and AN3661

(A) Multiple sequence alignment of CPSF3 proteins from *T. gondii* (*Tg*), *C. hominis* (*Ch*), *P. falciparum* (*Pf*), and CPSF73 of *H. sapiens* (*Hs*). The domain architecture is indicated as follows: blue, metallo-β-lactamase; green, β-CASP; orange, RNA specificity domain; magenta, the insertion within the MBL domain of apicomplexan parasites. Residues mutated in drug-resistant parasites are indicated by asterisks. The highly conserved residues involved in the coordination the zinc atoms Zn1 or Zn2 are indicated in gray. Mutations identified in parasites resistant to AN13762 or AN3661 are indicated in red and blue text, respectively.

Figure 4. Continued

(B) Schematic of *Cryptosporidium hominis* CPSF3/AN3661 co-crystal structure and modeling with AN13762. CPSF3 is displayed in a cartoon fashion with the same domain color code as in (A) surrounded by a light gray surface representation. Catalytic zinc atoms and coordinating residues are shown in gray sticks, whereas resistant mutations are shown in yellow and pink spheres.

(C) Zoom into the catalytic pocket with AN13762 manually placed colored in cyan.

(D) Zoom into the catalytic pocket binding AN3661 colored in dark purple.

resistance depends not only on the activity of Prodrug Activation and Resistance Esterase (PfPARE), an enzyme responsible for AN13762 processing, but also on enzymes involved in ubiquitination and SUMOylation pathways or PfCPSF3. The latter is responsible for the high level of resistance, thus suggesting that AN13762 or its refined derivative theoretically targets CPSF3 in malaria parasites as well. Whether AN13762 is processed in *T. gondii* is not known. However, as TgCPSF3^{G456S} selectivity toward AN13762 is based on steric hindrance over the methylazetidide group, which is cleaved off upon processing by the esterase, it seems unlikely that such a modification occurs in *T. gondii*. Note that no mutations with significant enrichment were found in TGGT1_306330, the closest homolog to PfPARE in *T. gondii* (Table S2). Furthermore, as AN13762 processing is required for full antimalarial activity, it is tempting to speculate that the lack of intracellular activation explains the decreased sensitivity observed in *T. gondii* and *Cryptosporidium* (EC₅₀ values are in the μM range, Figures 1C and 5B) relative to *P. falciparum* (EC₅₀ values ranging from 18 to 118 nM, Sindhe et al., 2020).

Based on the catalytic core sequence homology between TgCPSF3 and CpCPSF3, both previously chemically validated targets for *Toxoplasma* and *Cryptosporidium* (Palencia et al., 2017; Swale et al., 2019), we successfully laid the groundwork for pathogen hopping. In this respect, AN13762 efficiently inhibits *C. parvum*, a species relevant to human health, *in vitro* and *in vivo* in mouse model of infection. These results appear to be even more important for the treatment of cryptosporidiosis, where druggable targets are scarce and there is a high demand for more efficient therapies. However, further work will be needed to demonstrate that AN13762 acts as a direct binder of the CpCPSF3 and inhibits its mRNA processing activity, thereby restricting the growth of parasites. The recent discovery of benzoxaborole-based chemistry has given rise to a series of compounds with great potential against various infectious agents, including trypanosomatids and apicomplexan parasites by targeting different molecular targets (De Rycker et al., 2018). Remarkably, multiple compounds with known or suspected anti-CPSF3 activity across different organisms share a similar benzoxaborole scaffold that could be a prerequisite to CPSF3 binding (Begolo et al., 2018; Lunde et al., 2019; Palencia et al., 2017; Wall et al., 2018). Interestingly, the oxaborole acoziborole can cross the blood-brain barrier (Nare et al., 2010), offering a therapeutic option to eradicate persistent *Toxoplasma* cysts that are resistant to most, if not all, medications currently prescribed.

Limitations of the Study

Although our study is reasonably clear about AN13762 targeting CPSF3 in *Toxoplasma* and its activity against *Cryptosporidium* parasites, it remains possible that the mechanism of action in the latter is different and depends on prodrug-activating enzyme(s) such as PfPARE as described in *Plasmodium* species. Hopefully, recent advances in *Cryptosporidium* genetics will make it possible to carry out such investigations and genetically validate the CpCPSF3 molecular target in this organism (Vinayak et al., 2020).

Resource Availability**Lead Contact**

Further information and requests for resources and reagents should be directed to and will be fulfilled by the Lead Contact, Alexandre Bougdour (alexandre.bougdour@inserm.fr).

Materials Availability

All unique materials generated in this study are available from the Lead Contact upon request.

Data and Code Availability

This study did not generate/analyze code.

The Illumina RNA-seq dataset generated during this study is available at NCBI GEO: GSE156685.

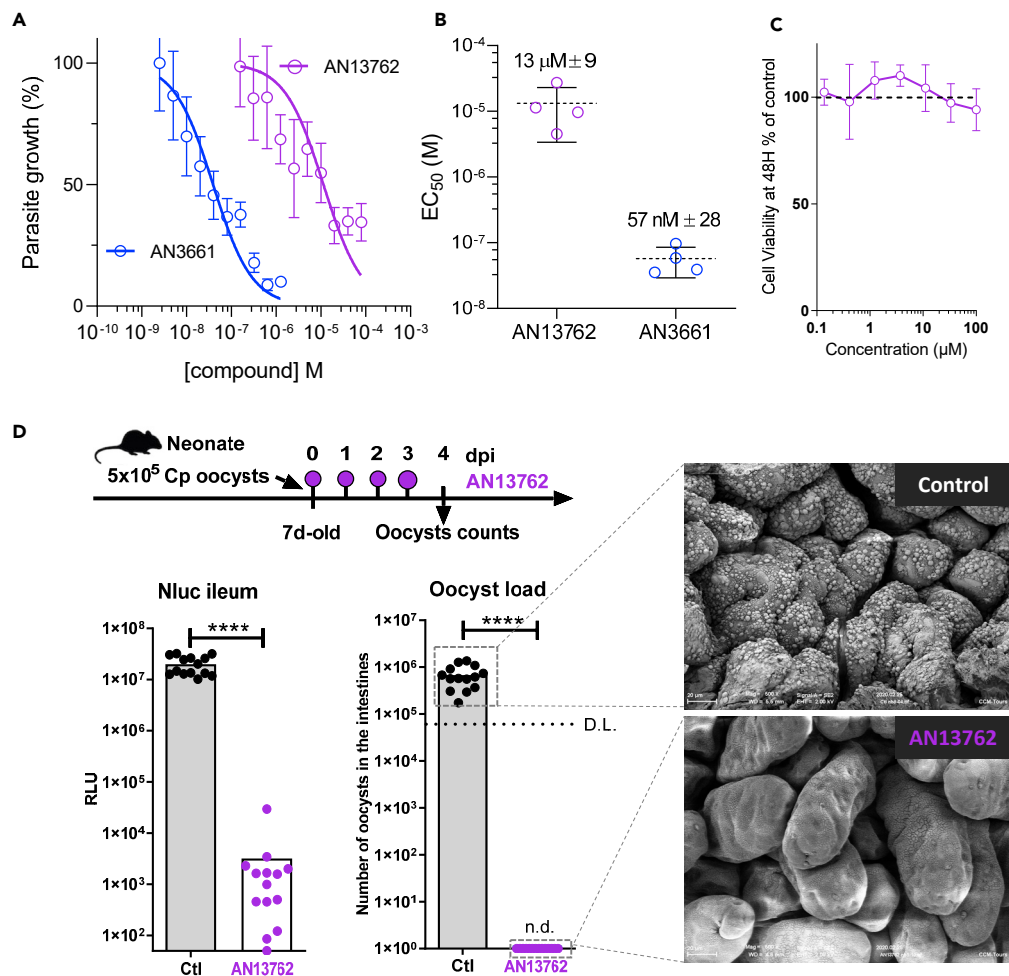


Figure 5. Efficacy Against *C. parvum* in Cell Culture and Neonatal Mouse Model

(A) Comparative inhibitory activity of AN13762 and AN3661 against *C. parvum* INRAE Nluc strain in human ileocecal HCT-8 cells. The effect of both drugs in reducing parasitic load in epithelial cells was monitored by the luminescence signal of transgenic Nluc parasites (each concentration point represents the average of six measurements ± SD.) Curves corresponding to AN13762 and AN3661 are in magenta and blue, respectively. Corresponding fluorescence microscopy images showing intracellular growth of *C. parvum* parasites can be found in Figure S5.

(B) Calculated EC₅₀ measurements are shown for AN13762 and AN3661 (n = 4 for each drug). Mean EC₅₀ values ± SD from 4 independent biological replicates are indicated.

(C) HCT-8 cell viability assay performed 48 h with increasing concentration of AN13762. Percent viability compared with the untreated control is displayed as a function of compound concentration in micromolar concentrations. Data are presented as mean ± SD of at least two independent biological assays. Dotted line represents 100% viability.

(D) Schematic representation of the 4-day oral dosage of AN13762 (40 mg/kg) in CMC from day 0 (4 h post-infection) in 7-day-old neonatal mice previously infected with 5 × 10⁵ oocysts. The degree of infection was monitored by counting the oocysts in the small intestine of the animals at 4 dpi (D.L., detection limit = 6 × 10⁴ oocysts/intestine) and by monitoring Nluc activity on a small piece of ileum of each neonatal mouse (n = 14 animals per group). n.d., not detected. Mann-Whitney test, ****P < 0.0001. Scanning electron microscopic imaging of neonatal mice ileum was performed at the end of the experiment on treated (AN13762) and mock treated (control) animals.

METHODS

All methods can be found in the accompanying [Transparent Methods supplemental file](#).

SUPPLEMENTAL INFORMATION

Supplemental Information can be found online at <https://doi.org/10.1016/j.isci.2020.101871>.

ACKNOWLEDGMENTS

We acknowledge A. Palencia for initial fruitful discussions. We thank D. Cannella and C. Corrao for technical assistance. This research was supported by funds from the Agence Nationale pour la Recherche Project ToxoP53 (grant no. ANR-19-CE15-0026) to A.B., Project HostQuest (grant no. ANR-18-CE15-0023), and the European Research Council (ERC Consolidator grant no. 614880 Hosting TOXO) to M.-A.H.

AUTHOR CONTRIBUTIONS

F.L., M.-A.H., and A.B. conceptualized the research. A.B. supervised the research. V.B. designed and conducted the *in vitro* studies performed in *T. gondii*. C.S. performed structural modelings. M.-P.B.-P. and V.B. designed and conducted the *in vivo* experiments with *T. gondii*. A.B. computed and analyzed the RNA-seq data. F.L. supervised the work performed on *Cryptosporidium*. T.P. realized the *in vitro* and *in vivo* studies performed with *Cryptosporidium*. S.G. performed the electron microscopy study. V.B., C.S., and A.B. wrote the manuscript. Funding Acquisition, M.-A.H. and A.B. All the authors contributed to the editing of the final version of manuscript, discussed, and approved the results.

DECLARATION OF INTERESTS

The authors declare no competing interests.

Received: August 17, 2020

Revised: October 27, 2020

Accepted: November 22, 2020

Published: December 18, 2020

REFERENCES

- Begolo, D., Vincent, I.M., Giordani, F., Pöhner, I., Witty, M.J., Rowan, T.G., Bengaly, Z., Gillingwater, K., Freund, Y., Wade, R.C., et al. (2018). The trypanocidal benzoxaborole AN7973 inhibits trypanosome mRNA processing. *PLoS Pathog.* 14, e1007315.
- De Rycker, M., Baragaña, B., Duce, S.L., and Gilbert, I.H. (2018). Challenges and recent progress in drug discovery for tropical diseases. *Nature* 559, 498–506.
- Dominski, Z., and Marzluff, W.F. (2007). Formation of the 3' end of histone mRNA: getting closer to the end. *Gene* 396, 373–390.
- Dunay, I.R., Gajurel, K., Dhakal, R., Liesenfeld, O., and Montoya, J.G. (2018). Treatment of toxoplasmosis: historical perspective, animal models, and current clinical practice. *Clin. Microbiol. Rev.* 31, e00057-17.
- Farrell, A., Coleman, B.I., Benenati, B., Brown, K.M., Blader, I.J., Marth, G.T., and Gubbels, M.-J. (2014). Whole genome profiling of spontaneous and chemically induced mutations in *Toxoplasma gondii*. *BMC Genomics* 15, 354.
- Lunde, C.S., Stebbins, E.E., Jumani, R.S., Hasan, M.M., Miller, P., Barlow, J., Freund, Y.R., Berry, P., Stefanakis, R., Gut, J., et al. (2019). Identification of a potent benzoxaborole drug candidate for treating cryptosporidiosis. *Nat. Commun.* 10, 2816.
- Lyons, S.M., Cunningham, C.H., Welch, J.D., Groh, B., Guo, A.Y., Wei, B., Whitfield, M.L., Xiong, Y., and Marzluff, W.F. (2016). A subset of replication-dependent histone mRNAs are expressed as polyadenylated RNAs in terminally differentiated tissues. *Nucleic Acids Res.* 44, 9190–9205.
- Manjunatha, U.H., Chao, A.T., Leong, F.J., and Diagana, T.T. (2016). Cryptosporidiosis drug discovery: opportunities and challenges. *ACS Infect. Dis.* 2, 530–537.
- Marzluff, W.F., Wagner, E.J., and Duronio, R.J. (2008). Metabolism and regulation of canonical histone mRNAs: life without a poly(A) tail. *Nat. Rev. Genet.* 9, 843–854.
- Nare, B., Wring, S., Bacchi, C., Beaudet, B., Bowling, T., Brun, R., Chen, D., Ding, C., Freund, Y., Gaukel, E., et al. (2010). Discovery of novel orally bioavailable oxaborole 6-carboxamides that demonstrate cure in a murine model of late-stage central nervous system African Trypanosomiasis. *Antimicrob. Agents Chemother.* 54, 4379–4388.
- Palencia, A., Bougdour, A., Brenier-Pinchart, M.-P., Touquet, B., Bertini, R.-L., Sensi, C., Gay, G., Vollaïre, J., Jossierand, V., Easom, E., et al. (2017). Targeting *Toxoplasma gondii* CPSF3 as a new approach to control toxoplasmosis. *EMBO Mol. Med.* 9, 385–394.
- Ross, N.T., Lohmann, F., Carbonneau, S., Fazal, A., Weihofen, W.A., Gleim, S., Salcius, M., Sigoillot, F., Henault, M., Carl, S.H., et al. (2020). CPSF3-dependent pre-mRNA processing as a druggable node in AML and Ewing's sarcoma. *Nat. Chem. Biol.* 16, 50–59.
- Ryan, K. (2004). Evidence that polyadenylation factor CPSF-73 is the mRNA 3' processing endonuclease. *RNA* 10, 565–573.
- Shi, Y., and Manley, J.L. (2015). The end of the message: multiple protein-RNA interactions define the mRNA polyadenylation site. *Genes Dev.* 29, 889–897.
- Sidik, S.M., Huet, D., Ganesan, S.M., Huynh, M.-H., Wang, T., Nasamu, A.S., Thiru, P., Saeij, J.P.J., Carruthers, V.B., Niles, J.C., and Lourido, S. (2016). A genome-wide CRISPR screen in *Toxoplasma* identifies essential apicomplexan genes. *Cell* 166, 1423–1435.e12.
- Sindhe, K.M.V., Wu, W., Legac, J., Zhang, Y.-K., Easom, E.E., Cooper, R.A., Plattner, J.J., Freund, Y.R., DeRisi, J.L., and Rosenthal, P.J. (2020). Plasmodium falciparum resistance to a lead benzoxaborole due to blocked compound activation and altered ubiquitination or sumoylation. *mBio* 11, e02640-19.
- Sonoiki, E., Ng, C.L., Lee, M.C.S., Guo, D., Zhang, Y.-K., Zhou, Y., Alley, M.R.K., Ahlyong, V., Sanz, L.M., Lafuente-Monasterio, M.J., et al. (2017). A potent antimalarial benzoxaborole targets a Plasmodium falciparum cleavage and polyadenylation specificity factor homologue. *Nat. Commun.* 8, 14574.
- Sun, Y., Zhang, Y., Aik, W.S., Yang, X.-C., Marzluff, W.F., Walz, T., Dominski, Z., and Tong, L. (2020). Structure of an active human histone pre-mRNA 3'-end processing machinery. *Science* 367, 700–703.
- Swale, C., Bougdour, A., Gnahoui-David, A., Tottey, J., Georgeault, S., Laurent, F., Palencia, A., and Hakimi, M.-A. (2019). Metal-captured inhibition of pre-mRNA processing activity by CPSF3 controls cryptosporidium infection. *Sci. Transl. Med.* 11, eaax7161.
- Vinayak, S., Jumani, R.S., Miller, P., Hasan, M.M., McLeod, B.I., Tandel, J., Stebbins, E.E., Teixeira, J.E., Borrel, J., Gonsse, A., et al. (2020). Bicyclic azetidines kill the diarrheal pathogen cryptosporidium in mice by inhibiting parasite

phenylalanyl-tRNA synthetase. *Sci. Transl. Med.* 12, eaba8412.

Wall, R.J., Rico, E., Lukac, I., Zuccotto, F., Elg, S., Gilbert, I.H., Freund, Y., Alley, M.R.K., Field, M.C., Wyllie, S., and Horn, D. (2018). Clinical and veterinary trypanocidal benzoxaboroles target CPSF3. *Proc. Natl. Acad. Sci. U. S. A.* 115, 9616–9621.

Zhang, Y.-K., Plattner, J.J., Easom, E.E., Jacobs, R.T., Guo, D., Freund, Y.R., Berry, P., Ciaravino, V., Erve, J.C.L., Rosenthal, P.J., et al. (2017). Benzoxaborole antimalarial agents. Part 5. Lead optimization of novel amide pyrazinyloxy benzoxaboroles and identification of a preclinical candidate. *J. Med. Chem.* 60, 5889–5908.

Zhao, S., Zhang, Y., Gamini, R., Zhang, B., and von Schack, D. (2018). Evaluation of two main RNA-seq approaches for gene quantification in clinical RNA sequencing: polyA+ selection versus rRNA depletion. *Sci. Rep.* 8, 4781.

iScience, Volume 23

Supplemental Information

Target Identification of an Antimalarial Oxaborole Identifies AN13762 as an Alternative Chemotype for Targeting CPSF3 in Apicomplexan Parasites

Valeria Bellini, Christopher Swale, Marie-Pierre Brenier-Pinchart, Tiffany Pezier, Sonia Georgeault, Fabrice Laurent, Mohamed-Ali Hakimi, and Alexandre Bougdour

Supplemental Information

Supplemental Figures

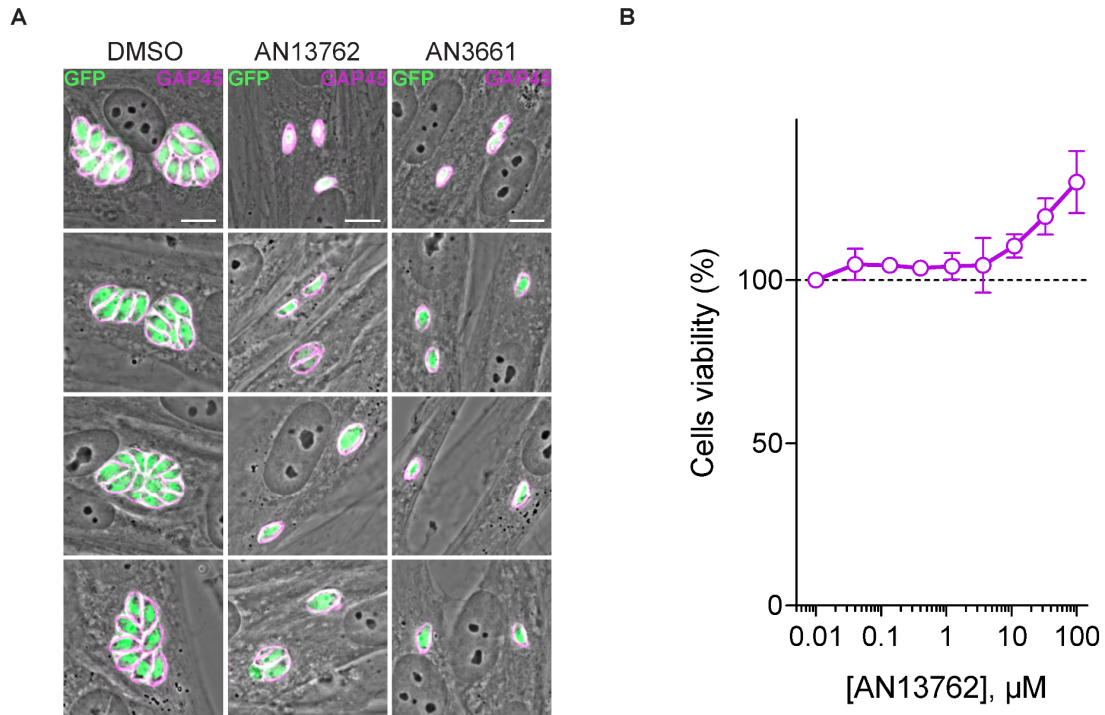


Figure S1. Activity of AN13762 against *Toxoplasma gondii*, Related to Figure 1. (A) Fluorescence microscopy showing intracellular growth of *T. gondii* parasites. HFF cells were infected with tachyzoites (RH $\Delta ku80$ UPRT::NLuc-P2A-EmGFP) and incubated with 10 μM AN13762, 5 μM AN3661 or 0.1% DMSO as control. Cells were fixed 24 h post-infection and then stained with antibodies against the *T. gondii* inner membrane complex protein GAP45 (magenta). The cytosolic GFP is shown in green. Scale bars represent 10 μm . (B) Effect of AN13762 on host-cell viability. HFF cells were incubated for 72 h in the presence of increasing concentrations of AN13762. Percent viability compared to the untreated control is displayed as a function of compound concentration in micromolar concentrations. Data are presented as mean \pm standard deviation (SD) of two independent biological assays, each with 3 technical replicates. Dotted line represents 100% viability.

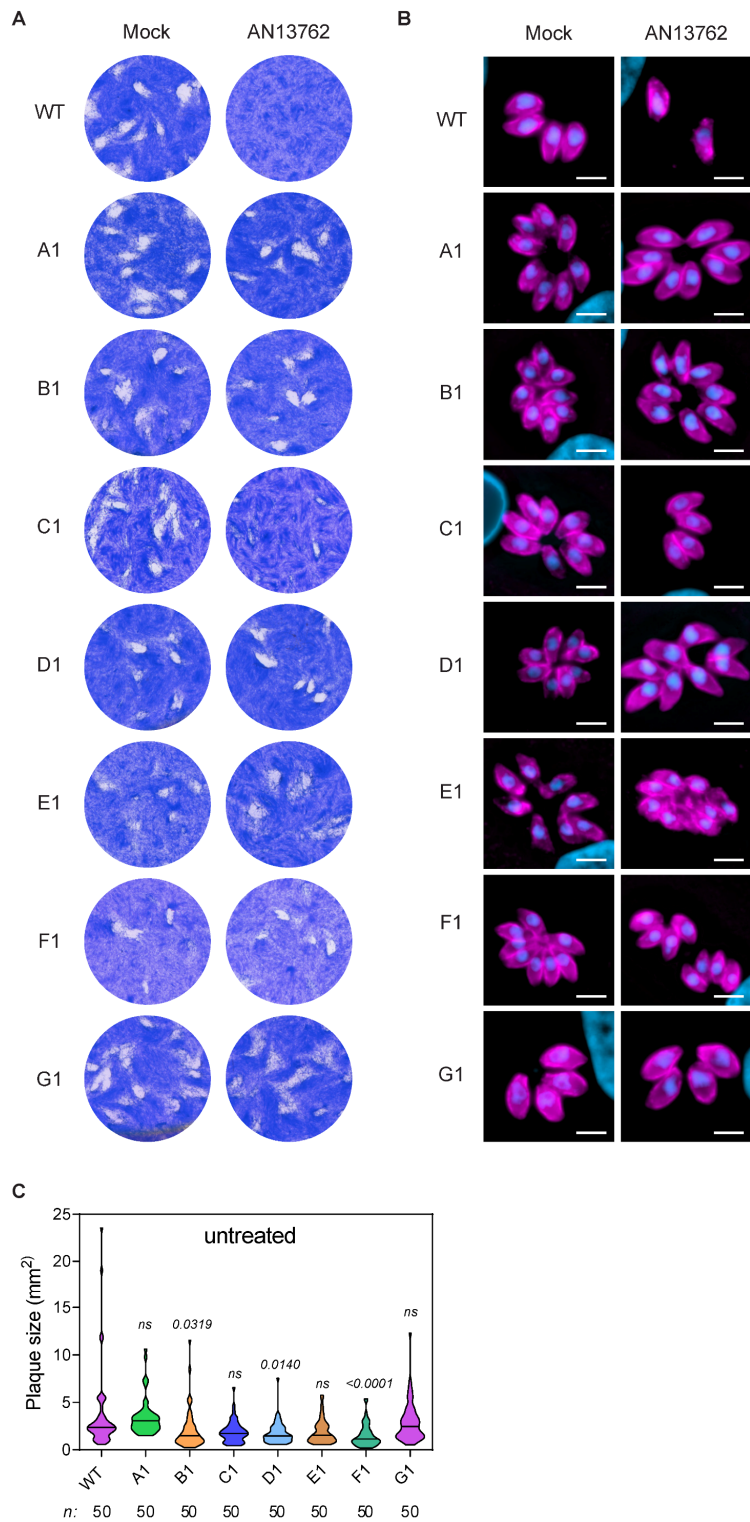


Figure S2. Activity of AN13762 against the EMS-induced drug-resistant lines, Related to Figure 2. (A) Plaque assay showing AN13762-resistant parasites forming plaques after 7 days of growth in the presence or absence of 10 μ M AN13762. (B) Fluorescence microscopy showing intracellular growth of *T. gondii* AN13762-resistant lines. HFF cells were infected by the indicated *T. gondii* strains in the presence or absence of 10 μ M AN13762. At 24 h post-infection, cells were fixed and stained with antibodies against GAP45 (magenta) and Hoechst (blue) to detect IMC of parasites and nuclei, respectively. (C) Quantification of plaque sizes shown in (A) when cultured in the absence of AN13762. *P*-values corresponding to Kruskal–Wallis test with Dunn’s multiple comparisons with the wild-type (WT) strain are indicated. *ns*, not significant.

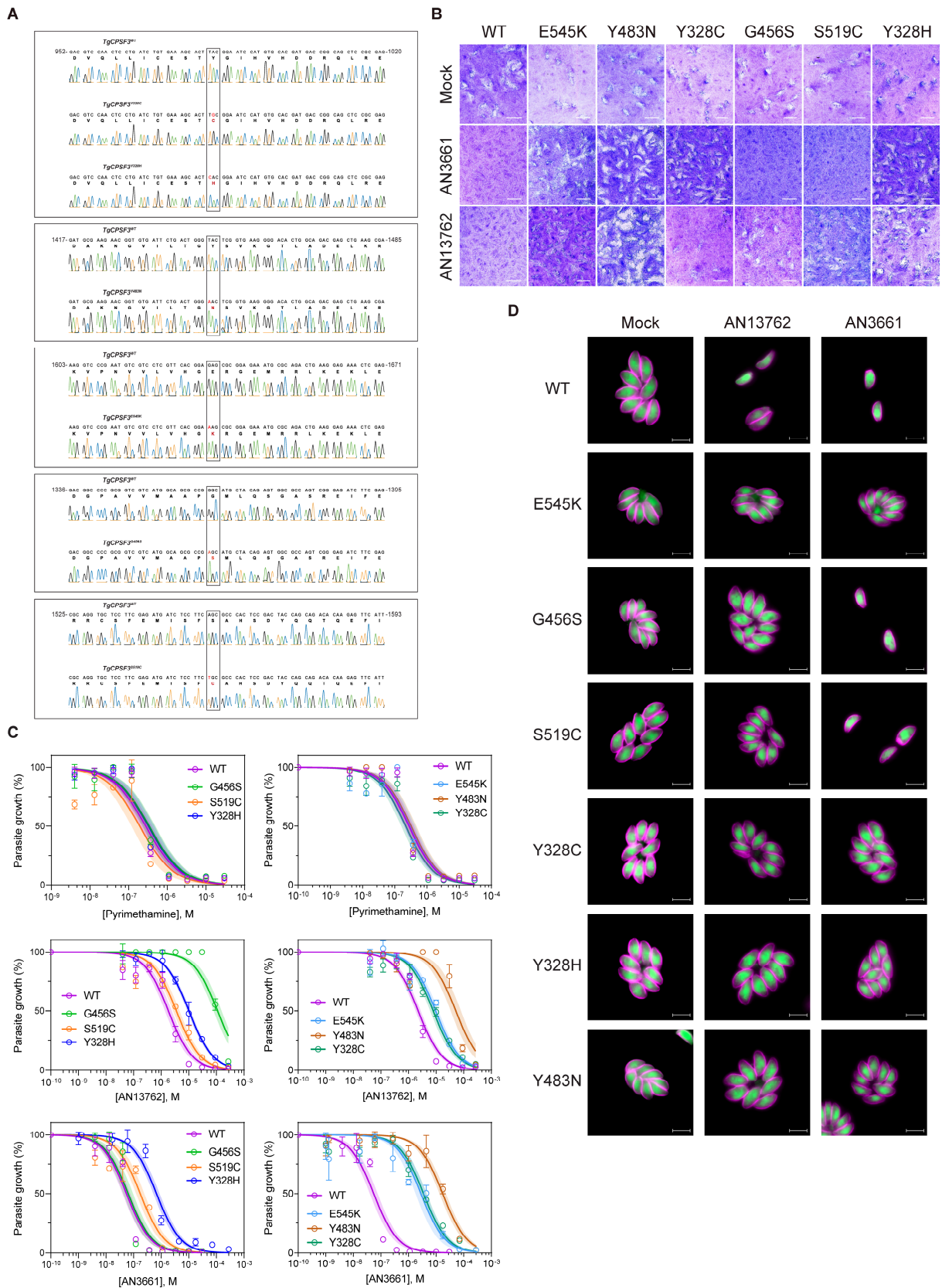


Figure S3. Activities of AN13762 and AN3661 against *CPSF3* edited parasites, Related to Figure 3. (A) Sanger chromatogram analysis showing *CPSF3* editing. Nucleotide positions relative to the ATG start codon on genomic DNA are indicated. (B) Effects of the compounds indicated on growth of the *CPSF3* edited parasites as assessed by plaque assay. Plaque sizes were measured after 7 days of growth in the presence or absence of 10 μ M AN13762 or 5 μ M AN3661. (C) Dose–response curves for

inhibition of *T. gondii* growth *in vitro* in response to increasing concentration of the indicated compounds. Confluent HFF monolayer were infected with WT and the engineered CPSF3 mutant strains (G456S, S519C, Y328H, E545K, Y483N, Y328C) expressing the NanoLuc luciferase. Data are presented as mean \pm standard deviation (SD) of n=3 technical replicates from a representative experiment out of at least two independent biological assays. Shaded error envelopes depict 95% confidence intervals. **(D)** Fluorescence microscopy showing intracellular growth of WT and the *CPSF3* edited parasites (G456S, S519C, Y328H, E545K, Y483N, Y328C). HFF cells were infected with tachyzoites of the indicated *T. gondii* strains expressing the *NLuc-P2A-EmGFP* reporter gene and incubated with 10 μ M AN13762, 5 μ M AN3661 or 0.1% DMSO as control. Cells were fixed 24 h post-infection and then stained with antibodies against the *T. gondii* inner membrane complex protein GAP45 (magenta). The cytosolic GFP is shown in green. Scale bars represent 10 μ m.

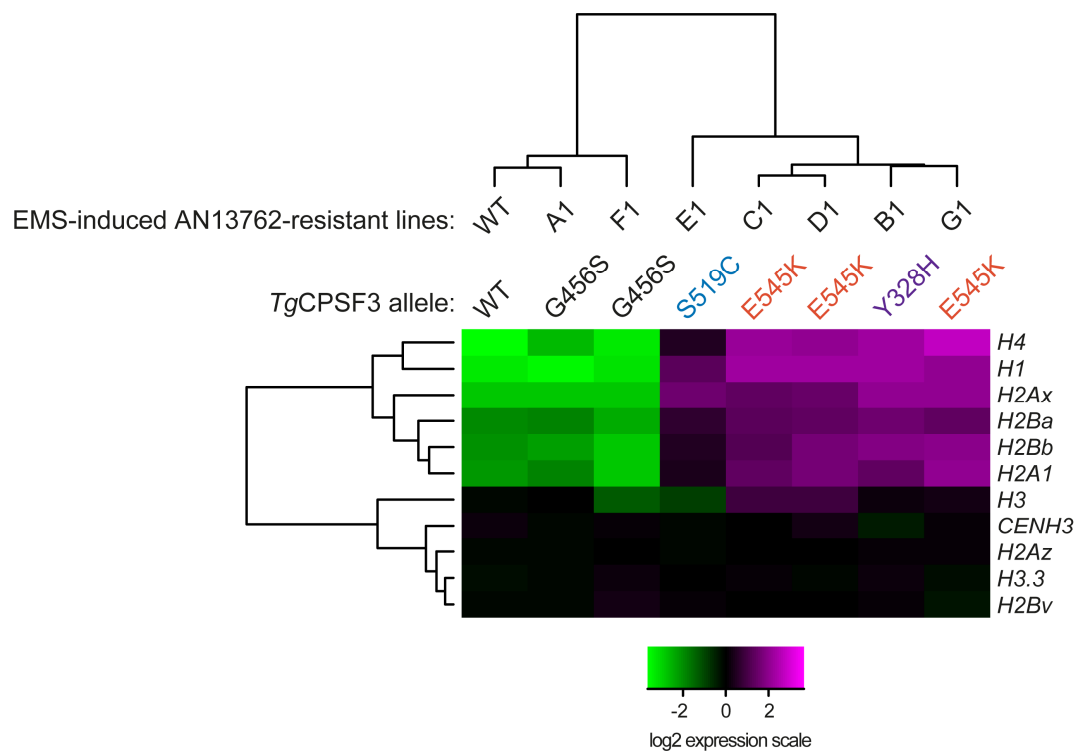


Figure S4. RNA-Seq analysis of genes encoding for histone subunits in WT and the EMS-induced AN13762-resistant strains (A1 to G1) of *T. gondii*, Related to Figure 2, Table S2, and Discussion. Heatmap of expression values obtained by RNA-Seq analysis of the indicated *T. gondii* genes. RPKM values were log₂ transformed and mean centered using iDEP.90 (Ge et al., 2018). Hierarchical clustering of the samples and the selected genes are shown on top and on the left, respectively.

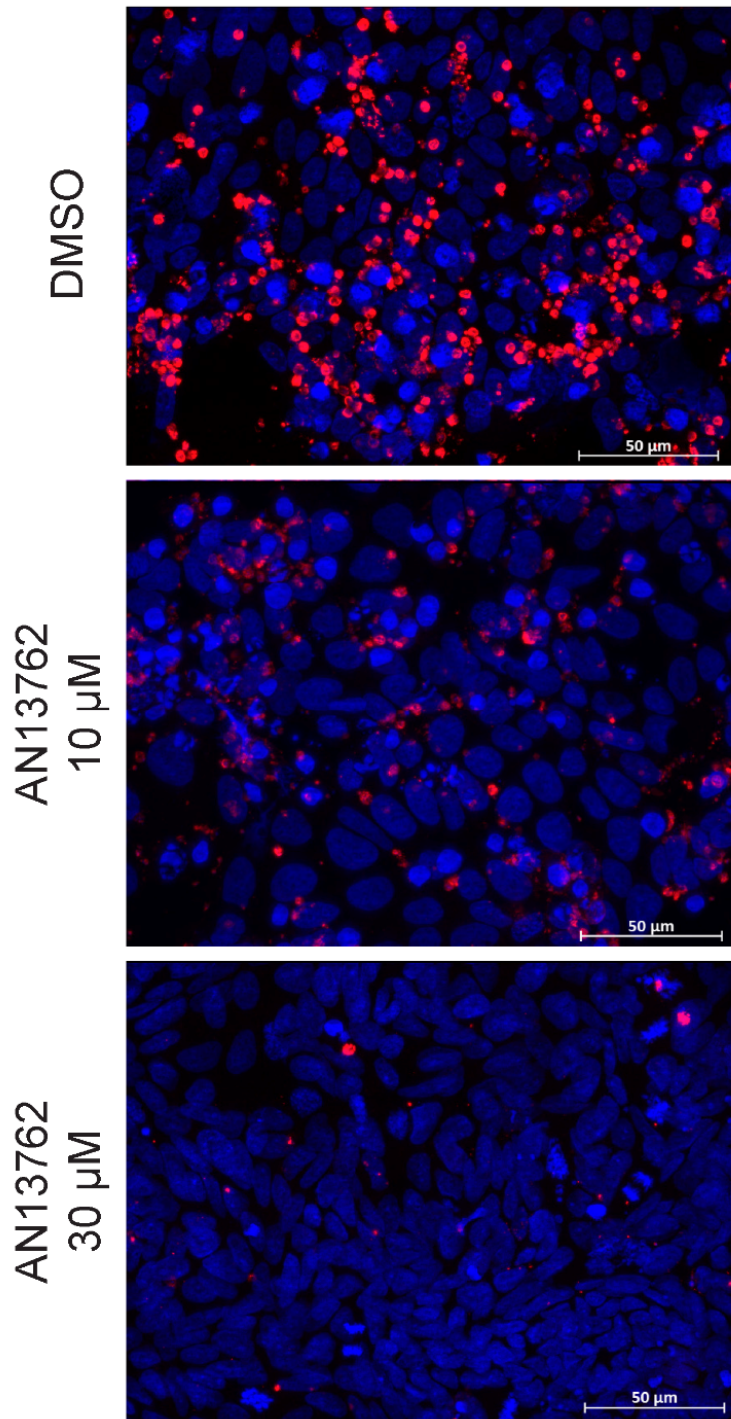


Figure S5. Activity of AN13762 against *Cryptosporidium parvum*, Related to Figure 5. Fluorescence microscopy showing intracellular growth of *C. parvum* parasites. Confluent HCT-8 cells were infected with freshly purified oocysts at a MOI of 1:1 of *C. parvum* INRAE Nluc strain in the presence of the indicated concentrations of AN13762 or 0.3% DMSO as control. Cells were fixed 48 h post-infection and then stained using rat antiserum generated against *C. parvum* (in red) and DAPI DNA-specific dye (in blue).

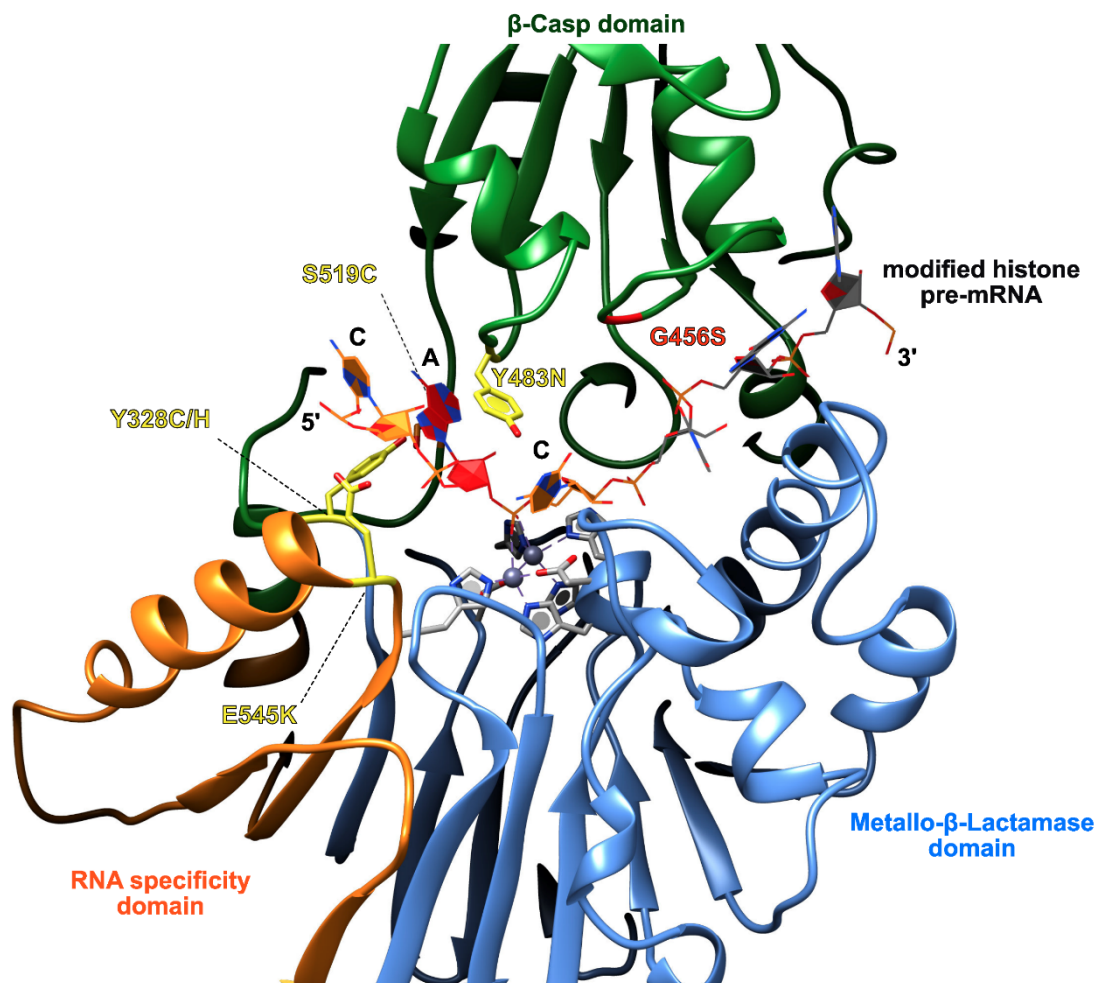


Figure S6. Oxaborole resistant mutations visualized within the human CPSF3 structure pre-catalytically bound to a modified histone H2A* pre-mRNA, Related to Figure 2 and Discussion. CPSF3 (extracted from the pdb-id: 6V4X) is displayed in cartoon fashion with the Metallo- β -Lactamase, β -Casp and RNA specificity domains colored respectively in blue, green and orange. Catalytic motif side chains are displayed in sticks and colored in grey. Mutated side chains conferring AN13762 and AN3661 resistance are shown as sticks and colored in yellow while the AN13762 exclusive resistant G456S is shown in red. Part of the modified H2A* histone pre-mRNA is displayed in a wire fashion with catalytic CAC cleavage motif bases highlighted in orange and red.

Transparent Methods

Parasite strains and cell culture

The *T. gondii* strains listed in the Table S1 were maintained by serial passage in HFF monolayers in Dulbecco's modified Eagle's medium (DMEM, Invitrogen) supplemented with 10% heat inactivated Fetal Bovine Serum (FBS) (Invitrogen), 10 mM (4-(2-hydroxyethyl)-1-piperazine ethanesulphonic acid) (HEPES) buffer pH 7.2, 2 mM L-glutamine, and 50 µg/mL of penicillin and streptomycin (Invitrogen). Cells were incubated at 37°C with 5% CO₂ in humidified air. Human ileocecal adenocarcinoma cells (HCT-8) cultured in RPMI 1640 with glutamine supplemented with 10% fetal bovine serum, 1 mM sodium pyruvate, penicillin (50 U/mL), and streptomycin (50 µg/mL).

Reagents

The compounds 6-(2-((3-hydroxy-3-methylazetidin-1-yl)carbonyl)pyrazinyl-5-oxy)-1,3-dihydro-1-hydroxy-7-methyl-2,1-benzoxaborole (AN13762) and 7-(2-carboxyethyl)-1,3-dihydro-1-hydroxy-2,1-benzoxaborole (AN3661) were purchased from ChemPartner (Purity ≥ 95% as determined by LC/MS, ¹H-NMR).

Plasmids and primers

Oligonucleotides were ordered from Sigma-Aldrich. PCR amplifications were performed with KOD Xtreme™ Hot Start DNA Polymerase. Primers and plasmids used or generated in this study are listed in Table S1.

The bicistronic vectors expressing the Cas9 genome editing enzyme and specific sgRNAs targeting the CPSF3 coding sequence were constructed as described previously (Curt-Varesano et al., 2016). Briefly, oligonucleotides CPSF3^{G456S}-CRISPR-FWD and CPSF3^{G456S}-CRISPR-REV, CPSF3^{Y328H}-CRISPR-FWD and CPSF3^{Y328H}-CRISPR-REV, and CPSF3^{S519C}-CRISPR-FWD and CPSF3^{S519C}-CRISPR-REV (Table S1) were annealed and ligated into the pTOXO_Cas9CRISPR plasmid to create vectors used for construction of *T. gondii* recombinant for CPSF3^{G456S}, CPSF3^{Y328H} and CPSF3^{S519C}, respectively.

Generation of a *T. gondii* strain expressing the NanoLuc bioluminescent protein

The construction carrying the Nluc-P2A-EmGFP coding sequences under the control of the *Tub8* promoter sequence (P_{Tub8}) was DNA-synthesized and cloned into pUC57-Simple vector by GenScript (DNA sequence provided in Table S1). Note that the P2A peptide sequence promotes a ribosomal skip, resulting in the stoichiometric expression of unfused Nluc and EmGFP reporter proteins from the same mRNA transcript. The P_{Tub8}-Nluc-P2A-EmGFP-3'UTR SAG1 cassette was amplified by PCR using primers HR-UPRT-P_{Tub8}_F and UPRT-SAG1-RH_R and targeted to the UPRT locus as previously described (Shen et al., 2014). Briefly, the resulting amplicon was co-transfected with the plasmid pTOXO_Cas9-CRISPR::sgUPRT (Farhat et al., 2020) for homology directed repair at the UPRT locus. Recombinant parasites were selected with 5 µM of 5-fluoro-2-deoxyuridine (FUDR) and clones expressing both Nluc and EmGFP were isolated by limiting dilution.

Immunofluorescence microscopy

Cells grown on coverslips were fixed in 3% formaldehyde for 20 min at room temperature, permeabilized with 0.1% (v/v) Triton X-100 for 5 min and blocked in phosphate buffered saline (PBS) containing 3% (w/v) BSA. Samples were incubated for 1 h with primary antibodies (rabbit anti-GAP45 kindly provided by Pr. Dominique Soldati, University of Geneva) followed by the addition of secondary antibodies conjugated to Alexa Fluor 488 or 594 (Molecular Probes) to detect intracellular parasites. Nuclei were stained for 10 min at room temperature with Hoechst 33258. Coverslips were mounted on a glass slide with Mowiol mounting medium, and 0.25 µm Z-images stacks were acquired with an Axio Imager M2 fluorescence microscope (Carl Zeiss, Inc.). Images were processed with Icy 2.0 (icy.bioimageanalysis.org) using the EpiDEMIC plugin for blind deconvolution of each channel, separately. Maximum projection of deconvoluted stack images are shown.

HCT-8 cells grown on glass coverslips were infected with *C. parvum* INRAE strain at MOI=1. Three hours later monolayers were washed carefully and cells further incubated for 48 h in presence of AN13762 at 10 or 30 µM or equivalent concentration of DMSO (0.3%). After gentle washing the wells were immediately fixed for subsequent DAPI and α-*C. parvum* polyclonal rat antiserum (followed by anti-rat alexa fluor 568 conjugate) staining.

Plaque assays

Freshly egressed parasites were inoculated on a confluent monolayer of HFFs and grown for 7 days with or without the indicated compounds. Cells were fixed and stained with Coomassie blue staining solution (0.1% Coomassie R-250 in 40% ethanol and 10% acetic acid as previously described (Curt-Varesano et al., 2016)).

***Toxoplasma gondii* in vitro measurement of EC₅₀**

The *in vitro* inhibitory activity of small compounds on *T. gondii* proliferation was determined as follows; 2,000 tachyzoites of *T. gondii* RH strain expressing the nanoluciferase (RH Nluc) were allowed to invade confluent HFF monolayer in a 96-well plate for 2h. Inhibitors (AN13762 and AN3661), along with pyrimethamine (minimum signal), were diluted in growth medium and added to the monolayers at various concentrations in triplicates (technical replicates) along with DMSO-treated controls (maximum signals). The assay was performed in a 100 μ L final volume. After 48 h of growth at 37°C, the medium was removed and 50 μ L PBS was added to each well. The NanoLuc assays were performed using the Nano-Glo® Luciferase Assay System according to manufacturer's instructions (Promega). Lysis was performed in the wells by adding 50 μ L Nano-Glo® Luciferase Assay Reagent containing 1:50th dilution of Nano-Glo® Luciferase Assay Substrate. After 3 minutes of incubation, luminescence was measured using the CLARIOstar® (BMG Labtech) plate reader. Bioluminescence values from the uninfected host cells was used to determine background signal. EC₅₀ were determined using non-linear regression analysis of normalized data and assuming a sigmoidal dose response. EC₅₀ values for each compound represent an average of at least two independent biological replicates. AN13762 cytotoxicity was assayed on HFF cells after 72 h of incubation using CellTiter-Blue Reagent® (Promega).

***Toxoplasma gondii* random mutagenesis**

Parasites were chemically mutagenized as previously described (Palencia et al., 2017), with the following modifications. Briefly, $\sim 10^7$ tachyzoites (RH strain) growing intracellularly in HFF cells in a T25 flask were incubated at 37°C for 4 h in 0.1% FBS DMEM growth medium containing either ethyl methanesulphonate (EMS, ranging from 2.5 to 7 mM final concentration) or the appropriate vehicle controls (Figure 2B). After exposure to mutagen, parasites were washed three times with PBS, and the mutagenized population was allowed to recover in a fresh T25 flask containing an HFF monolayer in the absence of drug for 3–5 days. Released tachyzoites were then inoculated into fresh cell monolayers in medium containing 10 μ M AN13762 and incubated until viable extracellular tachyzoites emerged 8–10 days later. Surviving parasites were passaged once more under continued AN13762 treatment and cloned by limiting dilution. Four cloned mutants were isolated each from 7 independent mutagenesis experiments. Thus, each flask contained unique SNV pools.

RNA-seq, sequence alignment, and variant calling

For each biological assay, a T175 flask containing a confluent monolayer of HFF was infected with RH wild-type or AN13762-resistant strains. Total RNAs were extracted and purified using TRIzol (Invitrogen, Carlsbad, CA, USA) and RNeasy Plus Mini Kit (Qiagen). RNA quantity and quality were measured by NanoDrop 2000 (Thermo Scientific).

RNA-sequencing was performed as previously described (He et al., 2018), following standard Illumina protocols, by GENEWIZ (South Plainfield, NJ, USA). Briefly, the RNA quality was checked with TapeStation System (Agilent Technologies, Palo Alto, California, USA), and Illumina TruSEQ RNA library prep and sequencing reagents were used following the manufacturer's recommendations (Illumina, San Diego, CA, USA). The samples were paired-end multiplex sequenced (2 x 125 bp) on the Illumina HiSeq 2500 platform and generated at least 40 million reads for each sample (Table S2).

The RNA-Seq reads (FASTQ) were processed and analyzed using the Lasergene Genomics Suite version 15 (DNASTAR, Madison, WI, USA) using default parameters. The paired-end reads were uploaded onto the SeqMan NGen (version 15, DNASTAR, Madison, WI, USA) platform for reference-based assembly and variant calling using the *Toxoplasma* Type I GT1 strain (ToxoDB-36, GT1 genome) as reference template. The ArrayStar module (version 15, DNASTAR, Madison, WI, USA) was used for normalization, variant detection and statistical analysis of uniquely mapped paired-end reads using the default parameters. The expression data quantification and normalization were calculated using the RPKM (Reads Per Kilobase of transcript per Million mapped reads) normalization method.

Variant calls were filtered to select variants present in coding regions with the following criteria: SNP% \geq 90%, variant depth \geq 30, and absent in the parental wild-type strain (Table S2). SNVs,

insertions and deletions present in regulatory or intergenic regions were filtered out as they are unlikely to contribute to drug resistance. Mutations were plotted on a Circos plot using Circa (OMGenomics.com).

***Toxoplasma gondii* genome editing**

Targeted genome modifications were performed using the CRISPR/Cas9 system as described previously (Palencia et al., 2017). The recombinant parasites harboring allelic replacement for *CPSF3*^{G456S}, *CPSF3*^{Y328H}, *CPSF3*^{S519C}, *CPSF3*^{Y328C}, *CPSF3*^{Y483N}, and *CPSF3*^{E545K} were generated by electroporation of the *T. gondii* RH NLuc strain with pTOXO_Cas9CRISPR vectors targeting the *CPSF3* coding sequence (sgCPSF3^{G456S}, sgCPSF3^{Y328H}, sgCPSF3^{S519C}, sgCPSF3^{Y328C}, sgCPSF3^{Y483N}, and sgCPSF3^{E545K}) and their respective donor single-stranded oligo DNA nucleotides (ssODNs) carrying respective nucleotide substitutions (*CPSF3*^{G456S}_donor, *CPSF3*^{Y328H}_donor, *CPSF3*^{S519C}_donor, *CPSF3*^{Y328C}_donor, *CPSF3*^{Y483N}_donor, and *CPSF3*^{E545K}_donor; Supplemental Table S1) for homology-directed repair. Recombinant parasites were selected with 10 µM AN13762 (*CPSF3*^{G456S}, *CPSF3*^{Y328H}, and *CPSF3*^{S519C}) or 5 µM AN3661 (*CPSF3*^{Y328C}, *CPSF3*^{Y483N}, and *CPSF3*^{E545K}), as described previously in (Palencia et al., 2017) prior to subcloning by limited dilution, and allelic replacement was verified by sequencing of *T. gondii* *CPSF3* genomic DNA.

***Toxoplasma gondii* in vivo mouse therapeutic assays**

All animal procedures were conducted under pathogen-free conditions in compliance with established institutional guidance and approved protocols from the European Directive 2010/63/EU. We used randomization and blinding to treatment assignment to reduce bias in mice selection and outcome assessment. Two independent experiments were performed with three mice in each treatment group (female CBA/JRj mice, Janvier, Le Genest-Dt-Isle, France; 7–9 weeks old). Mice were infected intraperitoneally with 10³ tachyzoites of the virulent type I RH NLuc strain and the RH NLuc *CPSF3*^{E545K} or *CPSF3*^{G456S} mutant strains. These inocula routinely resulted in high mortality in control mice at 6–12 days post-infection. Treatments were initiated at day 1 post-infection and were continued for seven consecutive days. Treated mice were orally administered 40 mg/kg AN13762 or 200 mg/kg sulphadiazine (Sigma), as previously described (Palencia et al., 2017), both suspended in 1% (w/v) carboxymethylcellulose (CMC, Sigma) and 0.1% (v/v) Tween-80 (Sigma). In surviving mice, the protective immunity acquired against *Toxoplasma* conferred after the first challenge was confirmed by a lethal secondary challenge with the RH NLuc strain (10³ tachyzoites per mouse).

***Cryptosporidium* EC₅₀ determination and cell toxicity**

The *in vitro* inhibitory activity of small compounds on *Cryptosporidium* and cell toxicity were determined as described previously (Swale et al., 2019). Briefly, confluent HCT-8 cells were infected with freshly purified oocysts (multiplicity of infection (MOI) of 1:1) of *C. parvum* INRAE NLuc strain in the presence of different concentrations of AN3661 or AN13762. After 3 h, cell cultures were washed twice, and media were replaced with the same compound concentration and further incubated for 24 or 48 h. Culture supernatant was removed from the wells (six replicates for each concentration), and 200 µl of Nano-Glo lysis buffer containing 1:50 of Nano-Glow substrate (Promega) was added to the wells. After 3 min of incubation, luminescence was measured with GloMax-Multi+ (Promega) and analyzed with Instinct software. EC₅₀ was determined from dose response inhibition curve using with GraphPad Prism software. AN13762 cytotoxicity was assayed on HCT-8 cells after 24 h of incubation using an MTS assay (CellTiter 96® AQueous One Solution Cell Proliferation Assay, Promega).

***Cryptosporidium* in vivo mouse therapeutic assays**

In vivo efficacy of AN13762 was assayed as described previously (Swale et al., 2019). Briefly, seven-day-old wild-type neonatal mice were infected by oral gavage with 5 × 10⁵ oocysts of *C. parvum* INRAE strain and treated orally with 20 µL of treatment suspension [40mg/kg] in CMC or sham treated with 20 µL of vehicle solution (CMC). The degree of infection in individual neonatal mice was assessed by determining the number of oocysts by coproscopy (Thoma counting chamber; detection limit of 6.10⁴ oocysts/small intestine) and NLuc activity in the intestinal contents.

Scanning electron microscopy

Ileal tissue samples were fixed by incubation for 24 h in 4% paraformaldehyde and 1% glutaraldehyde in 0.1 M phosphate buffer (pH 7.3). Samples were then washed in phosphate buffer, postfixed by incubation with 2% osmium tetroxide for 1 h, fully dehydrated in a graded series of ethanol solutions, and dried in hexamethyldisilane. Last, samples were coated with 40-Å platinum using a

GATAN PECS 682 apparatus before observation under a Zeiss Ultra plus FEG-SEM scanning electron microscope.

Homology modelling of *T. gondii* CPSF3 mutations and docking analysis of AN13762

Homology modelling visualization of the *T. gondii* CPSF3 mutated residues was performed using the *Cryptosporidium hominis* CPSF3/AN3661 co-crystal structure (pdb id: 6Q55) as a structural model basis. *T. gondii* point mutations were depicted through direct sequence conservation while AN13762 docking was performed by manual placement of the oxaborole core onto the AN3661 backbone in Coot ([Emsley et al., 2010](#)) with no further energy minimization performed. Schematics were produced using Pymol (Schrödinger, LLC) and UCSF Chimera.

Data and Code Availability

The accession number for the RNA-Seq data reported in this paper is GEO: GSE156685.

Supplemental References

Curt-Varesano, A., Braun, L., Ranquet, C., Hakimi, M.-A., Bougdour, A., 2016. The aspartyl protease TgASP5 mediates the export of the *Toxoplasma* GRA16 and GRA24 effectors into host cells: TgASP5 is essential for GRA16 and GRA24 export. *Cellular Microbiology* 18, 151–167.

Emsley, P., Lohkamp, B., Scott, W.G., Cowtan, K., 2010. Features and development of *Coot*. *Acta Crystallogr D Biol Crystallogr* 66, 486–501.

Farhat, D.C., Swale, C., Dard, C., Cannella, D., Ortet, P., Barakat, M., Sindikubwabo, F., Belmudes, L., De Bock, P.-J., Couté, Y., Bougdour, A., Hakimi, M.-A., 2020. A MORC-driven transcriptional switch controls *Toxoplasma* developmental trajectories and sexual commitment. *Nat Microbiol* 5, 570–583.

Ge, S.X., Son, E.W., Yao, R., 2018. iDEP: an integrated web application for differential expression and pathway analysis of RNA-Seq data. *BMC Bioinformatics* 19, 534.

He, H., Brenier-Pinchart, M.-P., Braun, L., Kraut, A., Touquet, B., Couté, Y., Tardieux, I., Hakimi, M.-A., Bougdour, A., 2018. Characterization of a *Toxoplasma* effector uncovers an alternative GSK3/β-catenin-regulatory pathway of inflammation. *Elife* 7.

Shen, B., Brown, K.M., Lee, T.D., Sibley, L.D., 2014. Efficient gene disruption in diverse strains of *Toxoplasma gondii* using CRISPR/CAS9. *MBio* 5, e01114–14.